Mon. Not. R. Astron. Soc. **000**, 1–27 (2006) Printed 10 February 2006 (MN LATEX style file v2.2)

The UKIRT Infrared Deep Sky Survey Early Data Release

S. Dye[1⋆], S. J. Warren[2], N. C. Hambly[3], N. J. G. Cross[3], S. T. Hodgkin[4], M. J. Irwin[4], A. Lawrence[3], A. J. Adamson[5], O. Almaini[6], A. C. Edge[7], P. Hirst[5], R. F. Jameson[8], P. W. Lucas[9], C. van Breukelen[10], J. Bryant[3], R. S. Collins[3], G. B. Dalton[10], J. I. Davies[1], C. J. Davis[5], D. W. Evans[4], S. Foucaud[6], E. A. Gonzales-Solares[4], P. C. Hewett[4], T. H. Kerr[5], S. K. Leggett[5], N. Lodieu[8], J. Loveday[11], J. R. Lewis[4], R. G. McMahon[4], D. J. Mortlock[2], Y. Nakajima[12], D. J. Pinfield[9], M. Rawlings[5], M. A. Read[3], M. Riello[4], K. Sekiguchi[13], A. J. Smith[11], E. T. W. Sutorius[3], W. Varricatt[5], S. J. Weatherley[2]

[1] *School of Physics & Astronomy, Cardiff University, 5 The Parade, Cardiff, CF24 3YB, U.K.*
[2] *Astrophysics Group, Imperial College London, Blackett Laboratory, Prince Consort Road, London, SW7 2AZ, U.K.*
[3] *Royal Observatory Edinburgh, Blackford Hill, Edinburgh, EH9 3HJ, U.K.*
[4] *Insitute of Astronomy, Madingley Rd., Cambridge, CB3 0HA, U.K.*
[5] *Joint Astronomy Centre, 660 N. A'ohoku Place, University Park, Hilo, Hawaii 96720, U.S.A.*
[6] *School of Physics and Astronomy, University of Nottingham, University Park, Nottingham, NG7 2RD, U.K.*
[7] *Department of Physics, Durham University, South Road, DH1 3LE, U.K.*
[8] *Department of Physics and Astronomy, University of Leicester, Leicester, LE1 7RH, U.K.*
[9] *Centre for Astrophysics Research, Science and Technology Research Institute, University of Hertfordshire, Hatfield, AL10 9AB, U.K.*
[10] *Department of Physics, Denys Wilkinson Building, Keble Road, Oxford, OX1 3RH, U.K.*
[11] *Department of Physics and Astronomy, University of Sussex, Brighton, East Sussex, BN1 9QH, U.K.*
[12] *National Astronomical Observatory of Japan, 2-21-1 Osawa, Mitaka, Tokyo, 181-8588, JAPAN*
[13] *Subaru Telescope, National Astronomical Observatory of Japan, 650 North A'ohoku Place, Hilo, HI 96720, U.S.A.*

Document in prep.

ABSTRACT

This paper defines the UKIRT Infrared Deep Sky Survey (UKIDSS) Early Data Release (EDR). UKIDSS is a set of five large near-IR surveys being undertaken with the UK Infra-red Telescope (UKIRT) Wide Field Camera (WFCAM). The surveys began in May 2005, and will last seven years. Each survey uses some or all of the broadband filter complement $ZYJHK$. The EDR is the first ESO-wide public release of data. All worldwide releases occur after a delay of 18 months from the ESO release. The EDR provides a small sample dataset (about 1% of the whole of UKIDSS) that is representative of the expected quality of future survey data releases. In addition an EDR+ dataset contains all EDR data, plus extra data of similar quality, but for areas not observed in all of the required filters. The first large data release, DR1, will occur in mid-2006. We provide details of the observational implementation, the data reduction, the astrometric and photometric calibration, and the quality control procedures. We summarise the data coverage and quality (seeing, ellipticity, photometricity, depth) for each survey and give a brief guide to accessing the images and catalogues from the WFCAM Science Archive.

Key words: astronomical data bases: surveys – infrared: general

1 INTRODUCTION

UKIDSS is the UKIRT Infrared Deep Sky Survey (Lawrence et al. 2006), carried out using the Wide Field Camera (WFCAM; Casali et al. 2006) installed on the United King-

⋆ E-mail: s.dye@astro.cf.ac.uk

© 2006 RAS

dom Infrared Telescope (UKIRT). Survey data acquisition started in May 2005. This paper defines the UKIDSS Early Data Release (EDR), the first release of UKIDSS data products to the ESO-wide astronomical community. The data were released on 10th February 2006, and are available from `http://surveys.roe.ac.uk/wsa`.

UKIDSS is a programme of five individual surveys that each use some or all of the broadband filter complement $ZYJHK$ (described by Hewett et al. 2006), and that span a range of areas and depths. There are three extra-galactic surveys; the Large Area Survey (LAS), the Deep Extra-galactic Survey (DXS), and the Ultra Deep Survey (UDS), covering complementary combinations of area and depth. Besides the LAS, there are two other wide surveys, aimed at targets in the Milky Way; the Galactic Plane Survey (GPS), and the Galactic Clusters Survey (GCS). The three wide, shallow surveys, LAS, GCS & GPS, use a total integration time of 40s per field per filter. The layout and filter complement of each survey are provided in Section 4. The complete UKIDSS programme is scheduled to take 7 years, requiring $\sim$1000 nights on UKIRT. The course of the full 7 year programme will be guided, to a certain extent, by the progress and scientific findings of the first two years of surveying. The design of these first two years consists of a set of fixed, shorter-term goals that define the '2–year plan'.

The purpose of the present paper is to provide a self–contained guide to the EDR. We have therefore included relevant background information extracted from the set of UKIDSS reference technical papers – on the surveys (Lawrence et al. 2006), the photometric system (Hewett et al. 2006), the camera (Casali et al. 2006), the data pipeline (Irwin et al. 2006), and the data archive (Hambly et al. 2006) – compressing details that will be the same for all data releases, and expanding on details that are specific to the EDR.

The outline of the paper is as follows: In the next section, we discuss the background to the UKIDSS programme. In Section 3, we provide a brief description of WFCAM, and in Section 4 we give an overview of the UKIDSS 2-year goals, in terms of area and filter coverage for each survey. We then follow the data-train sequence. In Section 5 we provide details of the observational implementation of the surveys, at a level that is required for understanding the data. For example this includes offsetting, microstepping, and stacking (i.e., averaging) strategies which dictate the structure of the image files. Section 6 describes the data reduction pipeline, and the procedures followed for the astrometric and photometric calibration of the data. The output from the pipeline is a set of reduced, stacked frames and associated catalogues of detected objects. After ingestion to the archive, the catalogues across different bands are merged. Section 7 describes the QC procedures applied to the UKIDSS EDR data, which takes place at two points. A series of checks are made on the individual frames. If a frame fails QC at this stage, the frame (or just the detector in that frame) and its catalogue are rejected. Catalogue merging is performed on data that pass the first QC stage, and a second stage of QC is executed on the merged catalogues. Data that pass both stages are prepared for release. The contents of the EDR are described in Section 8, where, in particular, plots of the distribution of the fields on the sky are provided. Access to the EDR is through the WSA, which is described in Section 9.

2 UKIDSS BACKGROUND

The design and implementation of the UKIDSS programme is the responsibility of the UKIDSS Consortium, an assemblage of astronomers with a common aim of completing the surveys. Observing is shared between UKIRT staff and UKIDSS astronomers. UKIDSS is an ESO public survey and UKIDSS consortium members have no proprietary data rights. Acquired data are shipped from UKIRT to the Cambridge Astronomical Survey Unit (CASU) at weekly intervals. At this stage, a copy of the raw UKIDSS data is sent from CASU to the ESO archive. At CASU, the data are processed by the WFCAM pipeline to produce stacked image data and source catalogues (see Section 6). The processed data products are electronically transferred to the Wide Field Astronomical Unit (WFAU) in Edinburgh where they are ingested by the WFCAM Science Archive (WSA; see Section 9). All WFCAM data, whether UKIDSS or not, follows the same route. UKIDSS, being the largest WFCAM user, has interacted closely on the design and development of the pipeline and archive.

Following commissioning of WFCAM a few nights (approximately 10 hours per survey) were devoted to science verification (SV) observations, in order to test the entire data train made up of the three elements: 1) the observational strategies employed by the different surveys (e.g., to check that integration times give background limited observations, offset patterns enable good sky correction and guide stars are sufficiently bright), 2) the processing steps executed by the WFCAM pipeline, from flatfielding and sky correction of the image data, to stacking and catalogue generation, 3) the functionality of the WSA, both archive ingest and source merging, and retrieval of the image and catalogue data through the web-based user interface (see Section 9). The SV data were analysed by UKIDSS consortium members, the results were fed back to CASU and WFAU, and the process was repeated after adjustments to the pipeline and archive. On the basis of the SV results, a set of quality control (QC) procedures for UKIDSS data was agreed (described in Section 7) which have then been applied to the EDR by WFAU. The SV dataset, much smaller than the EDR, is mostly heterogeneous. With the exception of some DXS data, the SV data have not been included in the EDR.

WFCAM is scheduled in blocks, a few months at a time, separated by intervals of a few months, and in such a way as to ensure that over a two-year span, access over the entire RA range is reasonably uniform. UKIDSS uses about 40% of all UKIRT time. The first WFCAM survey block, hereafter 05A, included UKIDSS survey observations over several nights commencing 13th May and ending 19th June 2005, and the second block, hereafter 05B, commenced 30th Aug 2005 and ended 25th January 2006. All data from 05A that passes QC is released here. The field of the deepest survey, the UDS (see Section 4), was not accessible in 05A. For this reason UDS data taken in 05B up to 30th September 2005, that satisfy QC, are also included in this release. Some changes to observing procedures, detailed in Section 5, were made between semesters 05A and 05B. Further changes are not anticipated.

The 05A data are somewhat inferior to the 05B data in terms of image quality and cosmetics. Correct alignment of the instrument requires that the instrument focal plane

assembly and optical focal plane are co-planar to within a small fraction of a milliradian. This can only be measured on sky, but requires disassembly of the instrument to adjust properly. An interim adjustment can be made by tilting the secondary mirror of the telescope as this results in a corresponding tilt of the optical focal plane, though this introduces other aberrations into the optics. The 05A data were taken with this type of interim adjustment in place and in good seeing, it is evident that the data are compromised by this. The instrument was opened up and the alignment corrected internally between the 05A and 05B observing blocks. Secondly, there is an issue of out–of–focus images of dirt on the field lens (see Section 7.2), which forms the end of the barrel of the instrument. Because the lens lies close to an intermediate focus, out–of–focus images of any dust or marks on the lens are visible in some frames. The top surface is frequently cleaned, while the bottom surface was cleaned in the interval between the 05A and 05B blocks to remove marks left by a lens handling jig, meaning, again, that the 05B data are superior.

The EDR dataset is relatively large compared to existing near-IR surveys (about as many photons have been collected as in 2MASS), and will be useful for science exploitation. However, compared to the whole of UKIDSS the EDR is only a small fraction, about 1%. From the UKIDSS perspective, the EDR is therefore a small prototype sample, released to the community as a stepping stone towards the goal of routine and prompt release of survey-quality data. We welcome feedback on the quality of the data and the functionality of the WSA. We aim to finalise the details of the data-train that define survey-quality products over early 2006, with further refinements of the pipeline, as well as adjustments and additions to the QC procedures. The entire 05A and 05B data will then be reprocessed for the first large data release, called DR1, scheduled for mid-2006. With this in mind, and considering the image quality and cosmetic issues of the 05A data, we have relaxed the QC criteria to a limited extent (e.g., depth and seeing), with the consequence that some fields included in the EDR will be excluded from DR1, and instead will be re-observed.

The EDR appears in the WSA as two databases. The EDR database is all the data where, for any pointing, the images and catalogues in all filters for that survey are available, and pass QC. The EDR+ database is all of the EDR data plus the remainder that passes QC, i.e., pointings where the full complement of filters for that survey is incomplete, either because some remain to be observed, or because some failed QC. In the remainder of the paper, where it is appropriate to make the distinction, we refer to the 'EDR database' and the 'EDR+ database'. The general term 'EDR' implies the combination. The extra content of the EDR+ database is very heterogeneous in terms of completeness of the filter complement, so that its usefulness is less apparent, considering that the surveys were designed around science goals that require the complete filter complement. We therefore anticipate that users will be most interested in the EDR database. Accessing the two databases is explained in detail in Section 9.

The first UKIDSS observations were made in May 2005, so that EDR represents a maximum lag of 9 months from acquisition to release. After finalisation of the pipeline and QC procedures, and automation of the latter, the time-lag will rapidly diminish. The intention is that by the end of 2006, the entire process, from acquisition to the data being publicly accessible in the WSA will be reduced to approximately 6 weeks. Accordingly, following DR1, UKIDSS will adopt a dual-layered data release policy. On the lower layer, new data will be released from the WSA unannounced at regular intervals. On the upper layer, official data releases will take place at intervals of each WFCAM block. Each official release will be accompanied by an announcement publication defining the specific data products included in that release.

3 WFCAM

WFCAM was built by the Astronomical Technology Centre (ATC) in Edinburgh as a common user instrument for UKIRT. The UKIDSS programme owes its feasibility to the large field of view of the camera. This section provides details of the design and construction of WFCAM, relevant for understanding the contents of the EDR, including some of the unusual properties of WFCAM data, as well as the characteristics peculiar to this release. We refer the reader to Casali et al. (2006) for full technical details of WFCAM.

The survey speed of an instrument is proportional to the telescope+instrument étendue[1]. At the time of writing, WFCAM's étendue of 2.38 m^2 deg^2 is the largest of any near-infrared imager in the world. The large field of view of WFCAM, 0.21 deg^2, is achieved with four Rockwell Hawaii-II 2048 × 2048 18μm-pixel array detectors, with a relatively large pixel scale of 0.4″. In good seeing the point spread function (PSF) is consequently under-sampled. Microstepping and interlacing allow sampling on scales of 1/2 or 1/3 of a pixel (see Section 5). The layout of the four detectors, and their numbering scheme is shown in Figure 1. The detectors cannot be butted because of their packaging. Instead they are spaced at 94% of the detector width, as shown. Four exposures are required to survey a contiguous area, referred to as a 'Tile' (see Section 5.1). As indicated in Figure 1, each detector is rotated by 90° with respect to its neighbours. The pixel x, y coordinate convention is indicated for the detectors.

Each detectors is divided into quadrants, and each quadrant is divided into eight channels of 128 × 1024 pixels. The channel packing relative to the xy axes is illustrated in Figure 1. The packing rotates through 90° in moving to an adjacent quadrant. This channel packing arrangement is visible for detector 4 in Figure 3.

The required pixel scale of 0.4″ corresponds to $f/2.4$ for UKIRT, and is close to that achieved at prime focus since UKIRT's primary is $f/2.5$. However there is insufficient room inside the small UKIRT dome for a large instrument at prime focus. The adopted design involves a new $f/9$ secondary, producing an intermediate focus 5.7m above the primary. A field lens is located at this point, and forms the end of the barrel of the instrument. The field lens images the primary mirror to a cold stop inside the cryostat, which baffles stray thermal emission. An ellipsoidal tertiary

[1] product of telescope collecting area, and solid angle of instrument field of view, sometimes called *grasp*

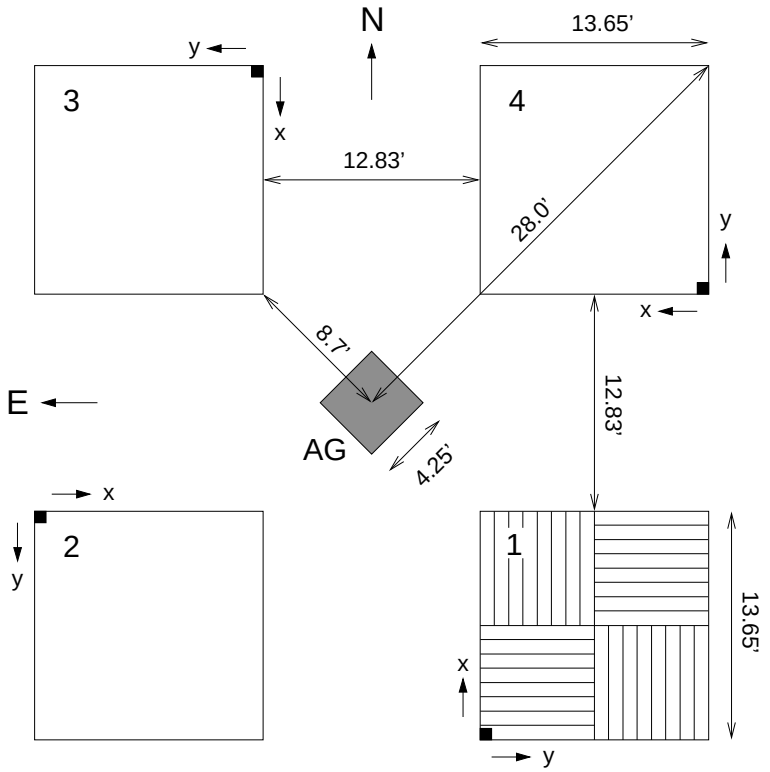

Figure 1. Layout of the WFCAM focal plane. Detector numbering follows that used in the WSA and is the same as the extension numbering in the FITS data files. Detectors are divided into four quadrants, each quadrant having 8 channels as illustrated in detector 1. The autoguider (grey shading) sits at the centre of the focal plane. North is up, East is left.

mirror, provides the f conversion, returning the beam upwards to the downward–looking focal plane. The autoguider is located on the optical axis, as shown. Because of the packaging of the Hawaii-II detectors, it was necessary to raise the guider CCD above the focal plane. This required mounting an auxiliary lens at the centre and just above the field lens, to raise the autoguider focal plane. This also changes the f-ratio to achieve the required pixel scale.

WFCAM has eight filter housings. Because the focal plane vignettes the beam, to minimise throughput loss the filters are stored vertically, rather than in a wheel. Consequently the detectors are exposed to unfiltered light when the filter is changed. Currently, the standard filter complement includes the broadband set $ZYJHK$, and two narrowband filters, H_2 1-0 S1 & Brγ. The eighth filter housing is blanked for darks. The WFCAM J, H and K bandpasses follow the specification of the Mauna Kea filter set (Tokunaga, Simons & Vacca 2002). The WFCAM Z filter has an effective wavelength of 0.87μm and the WFCAM Y filter fills the gap between Z and J. The system throughput, above-atmosphere-to-detector, is close to 20% at J, slightly higher at H and K, and slightly lower at Z and Y. The $ZYJHK$ photometric system of the instrument has been characterised by Hewett et al. (2006), who provide the total system response curves for each broad band, as well as colour equations to translate to 2MASS J, H, K (see also Section 6.4) and SDSS z, and synthetic colours of a wide variety of stars, galaxies and quasars .

UKIDSS observations are made in one of two read modes. In correlated double sampling (CDS), after a detector reset, an initial read is made, followed by an integration of the desired length, followed by a final read. The resulting output is the difference of the two reads. CDS has higher read-noise $\sim 30e^-$, but smaller overhead. CDS is used for all UKIDSS JHK observations, which use shorter integrations because of the high background. In non-destructive read (NDR) mode, after the detector reset, several reads sample the build up of charge throughout the integration, and the counts are established by a linear fit. NDR has lower read-noise $\sim 20e^-$, but larger overhead. NDR is used for all ZY observations, which use longer integrations, to achieve sky-noise limited performance.

The detectors are of PACE manufacture. The frames exhibit four characteristics that are unwelcome: pixel covariance, curtaining, persistence, and cross-talk. *Pixel covariance* is a result of inter-pixel capacitance. The result is that the pixel to pixel variance is reduced by a factor of about 1.2, and that the readout gain (photons per ADU) is overestimated by this factor when computed in the traditional way using photon–noise transfer curves. In this paper, where appropriate, e.g., in computing the system throughput, we have compensated for the effect. *Curtaining* is a rapidly varying constant bias offset along each 'line', where the pattern repeats in each quadrant (rotating in the same manner as the channel packing). The term 'line' here means 1024 pixels along the direction of the short axis of the channels. The pattern fluctuates with an RMS of $\sim$3 ADU and is completely random; no two detector frames are ever affected in the same way. *Persistence* is the effect of image latency whereby counts from a bright source are not completely re-

moved after a detector reset. Artificial images of sources can also occur due to cross-talk between the detector channels within a quadrant. Persistence and cross-talk are described in Section 6, and at greater length by Irwin et al. (2006).

4 THE UKIDSS 2-YEAR PLAN

The design and layout of the surveys are set out in Lawrence et al. (2006) which is the reference work for details of the final (7-year) goals of the UKIDSS programme. These goals are summarised in Table 1, in terms of areas, filters, number of passes, and (final summed) depth. All depths quoted in this paper are in the Vega photometric system, and correspond to the total brightness of a point source for which the summed flux in a 2″ diameter aperture has, on average, S/N= 5. The original designed depths were based on a first estimate of sensitivities in each band, made in 2001 and later revised downwards. It is apparent from analysis of the EDR dataset that the achieved sensitivities are indeed less deep than the original estimates, by an average of 0.2 mag. In light of this, all target depths have been adjusted by 0.2 mag and these are the values quoted here and in Lawrence et al. (2006). The overestimate of the detector quantum efficiency, due to pixel covariance (Section 3), is the main contribution to the overestimate of the instrument throughput.

In each of the shallow surveys, the depth in a select filter (J for LAS, K for GCS, GPS) is built up in two or three passes, in order to provide proper motions and variability information. Thus any field is observed in the full filter complement at one epoch and observed in the select filter only at one or two other epochs. The repeat passes are separated by a minimum of two years, to provide a sufficient baseline for measurement of proper motions. For scheduling reasons, in some areas the first epoch is with the full filter complement, and in other areas the first epoch is with the select filter.

The surveys are currently focused on completing a set of goals for the first two years of operations, hereafter referred to as the 2-year plan. In this section we describe the 2-year plan, which provides the context of the EDR and explains, for example, why some areas are covered in only a single band. In the 2-year plan the LAS and GCS are accelerated relative to the other surveys.

Table 2 summarises the relevant details of the 2-year plan for each survey, listing area to be surveyed, filter, target depth, and default integration time, for the shallow surveys, for good conditions. As explained in Section 5, in cases of mediocre seeing, bright sky, or thin cirrus, observations in some fields are still undertaken, but the integration times are increased, to ensure the target depth is achieved. The geometry of the target areas in the 2-year plan is shown in Figure 2. In what follows, we provide additional details of the 2-year plan, describing each survey in turn. Section 8 describes the data contents of the EDR.

Survey	Area (deg^2)	Filter	No. passes	Depth
		Y	1	20.3
LAS	4028	J	2	19.8
		H	1	18.6
		K	1	18.2
	1868	J	1	19.8
GPS	1868	H	1	18.9
	1868	K	3	18.8
	300	H_2	3	...
		Z	1	20.4
		Y	1	20.3
GCS	933	J	1	19.5
		H	1	18.6
		K	2	18.5
	35	J	multiple	22.3
DXS	5	H	multiple	21.8
	35	K	multiple	20.8
		J	multiple	24.8
UDS	0.77	H	multiple	23.8
		K	multiple	22.8

Table 1. Summary of the final (7-year) goals of the UKIDSS programme. Depth is 5σ for a point source.

Survey	Area (deg^2)	Filter	Depth	t_{int}
	2120	Y	20.3	40s
LAS	3120	J	19.5	40s
	2120	H	18.6	40s
	2120	K	18.2	40s
	338	J	19.8	80s
GPS	338	H	18.9	80s
	1868	K	18.2	40s
	300	H_2	...	150s
	234	Z	20.4	40s
	234	Y	20.3	40s
GCS	234	J	19.5	40s
	234	H	18.6	40s
	604	K	18.2	40s
	12.6	J	22.3	
DXS	12.6	K	20.8	
	0.77	J	23.8	
UDS	0.77	K	22.8	

Table 2. Summary of the goals of the UKIDSS 2-year plan. Depth is 5σ for a point source. For the shallow surveys the default integration time for normal conditions is listed. Some fields are observed in mediocre conditions, as detailed in Section 5.

4.1 LAS 2-year plan

The LAS is made up of 3 blocks, visible in Figure 2. All three blocks lie within the SDSS footprint. In the southern Galactic hemisphere there is an equatorial stripe, Block 1, of area 212 deg^2. In the northern Galactic hemisphere, there is an equatorial block, Block 2, and a block at higher declinations, Block 3, both of area 1908 deg^2. The LAS 2-year plan is to survey Block 1 and Block 2 in a single pass in $YJHK$. In addition, depending on conditions (Section 5), part of Block 3, an estimated 1000 deg^2, will be covered in a single pass in J only. For scheduling purposes each block has been subdivided into regions. The EDR contains data

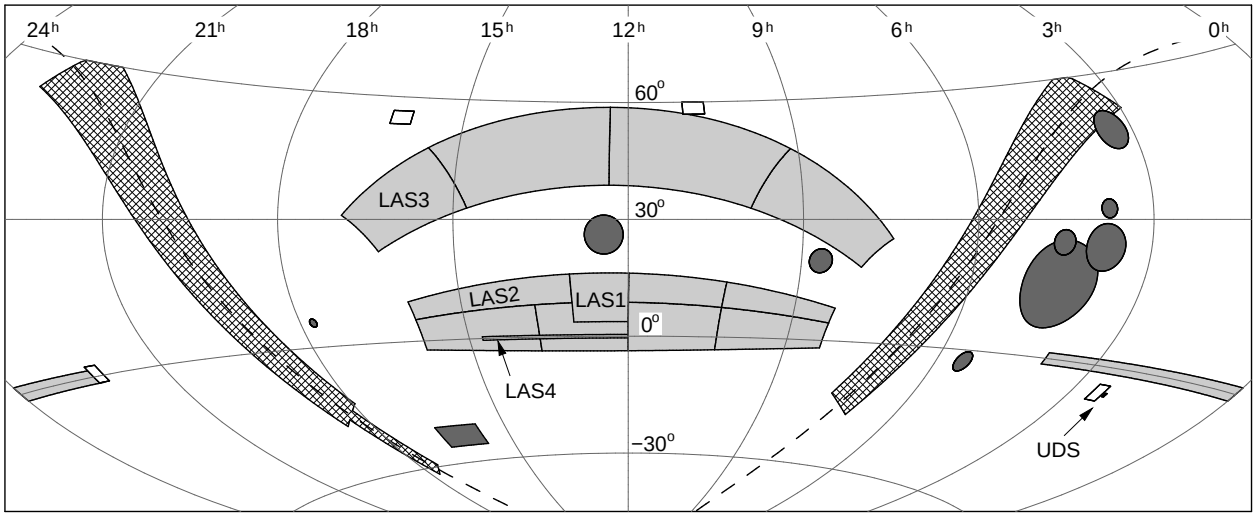

Figure 2. The UKIDSS 2 year plan survey areas showing the LAS (solid light grey), GPS (cross-hatched), GCS (solid dark grey), DXS (empty squares) and UDS (as labelled, lying alongside the western-most DXS field). The dashed line indicates the Galactic plane. Note that in the 2-year plan the LAS northern block receives J only coverage and most of the GPS areas shown receive K only (see text).

from the regions marked LAS1, LAS2, LAS3 & LAS4 (see Section 8).

4.2 GPS 2-year plan

The GPS will cover the band of Galactic latitude $|b| < 5°$, that lies within the declination range $-20° < \delta < +60°$. This translates to two blocks defined by the Galactic longitude ranges $15° < l < 107°$ and $142° < l < 230°$. In addition there will be a thin extension into the Galactic Centre, defined by $|b| < 2°$, $-2° < l < 15°$, as well as imaging of the Taurus-Auriga-Perseus star-formation complex in the H_2 narrow–band filter only.

The fields for the first two years are illustrated in Figure 2, and concentrate on the region of the inner Galaxy, close to the plane. The region $|b| < 1°$ in the longitude range $-2° < l < 107°$ will be imaged in JHK. This includes the area covered by the northern half of the GLIMPSE survey (Churchwell et al. 2002) using the Spitzer Space Telescope. Also, the block covering $30° < l < 45°$ will be imaged in JHK, over the remainder of the full thickness, $|b| < 5°$. The whole of the remainder of the GPS area, defined at the top, will be surveyed in K only. Finally the first pass of the H_2 imaging of the ~ 300 deg^2 Taurus-Auriga-Perseus star-formation complex will be completed (shown as the dark grey rectangle in Figure 2). For more information and details of updates, we refer the reader to the GPS web site located at *http://star-www.herts.ac.uk/∼pwl/UKIDSS_GPS.html.*

4.3 GCS 2-year plan

The GCS will observe the 10 star clusters listed in Table 3. These are ranked by priority, which gives an indication of the sequence in which they will be completed. In the 2-year plan, five of the clusters will be completed in all filters, as well as the central regions of three other clusters, as listed in the table. In addition the two remaining clusters will be covered in K only.

Field	Type	RA, Dec	Filters	Area (deg^2)
IC 4665	OC	17:46,+05:43	$ZYJHK$	0.8
Pleiades	OC	03:47,+24:07	$ZYJHK$	79
Alpha Per	OC	03:22,+48:37	$ZYJHK$	50
Praesepe	OC	08:40,+19:40	$ZYJHK$	28
Tau.-Aur.	SFA	04:30,+25:00	$ZYJHK$	cen. 24
Orion	SFA	05:29,−02:36	$ZYJHK$	cen. 16
Sco	SFA	16:10,−23:00	$ZYJHK$	cen. 24
Per-OB2	SFA	03:45,+32:17	$ZYJHK$	12.6
Hyades	OC	04:27,+15:52	K only	291
Coma-Ber	OC	12:25,+26:06	K only	78.5

Table 3. The GCS fields, with details of coverage in the 2-year plan. Types are open cluster (OC) or star formation association (SFA)

For the GCS the EDR contains data from the Sco and Coma-Ber clusters. For more information and details of updates, we refer the reader to the GCS web site located at *http://www.roe.ac.uk/∼nch/gcs/.*

4.4 DXS 2-year plan

The DXS comprises 12 contiguous Tiles in each of four fields; XMM-LSS (2^h25^m,$-4°30'$), ELAIS N1 (16^h10^m,$+54°00'$), the Lockman Hole (10^h57^m,$+57°40'$) and VIMOS 4 (22^h17^m,$+0°20'$). The 2-year plan is to reach full depth in four Tiles in J and K in each of the four fields. Rather than build up depth over all four Tiles, the strategy is to achieve target depth in one Tile before moving on to the next.

4.5 UDS 2-year plan

The UDS is a single 0.8 deg^2 Tile, centred on 2^h18^m,$-5°10'$, chosen to coincide with the Subaru/XMM-LSS field. This field lies just westwards of the XMM-LSS field in the DXS. The 2-year plan is to cover the Tile to $K = 22.8$, i.e., full

depth, and to $J = 23.8$, i.e., one magnitude short of full depth.

5 SURVEY OBSERVATIONAL IMPLEMENTATION

In this section we set out relevant details of the observational implementation that are needed for understanding the characteristics of the data. These include, for example, whether microstepping was employed. The observing procedures were adjusted in the interval between 05A and 05B.

5.1 General details

Observations are packaged in 'minimum schedulable blocks' (MSBs). MSBs typically last one hour, and are designed to be self contained in the sense that the sky frames for sky subtraction may be formed from the data itself. Each MSB has its own set of criteria for the conditions under which it may be executed. At the summit the UKIRT observing management program automatically schedules MSBs according to their observability (i.e. hour angle and airmass), and the current conditions (transparency, seeing, J-band sky brightness).

The basic unit of the surveys is the stack multiframe, which is the group of four images, one for each detector, formed by averaging the set of exposures made at the same base position within a given MSB. The region being surveyed is tessellated by these stack multiframes. The smallest contiguous region that can be surveyed is a Tile, requiring four base positions to fill in a solid angle of 0.77 deg^2.

Descriptions of the implementation of each survey employ the following observing terminology, defined by UKIRT, which we use with appropriate capitalisation to distinguish from the general term:

- *Exposure* - An Exposure is a single complete cycle of the detector readout mode, over a time specified as the Exposure Time, $t_{\rm exp}$ (referred to by the `expTime` attribute in the WSA).
- *Integration* - An Integration is a sequence of one or more Exposures, that are averaged by the data acquistion system, resulting in a single image being written to disk. An Integration is therefore the basic observational product. For all UKIDSS observations, Integrations comprise single Exposures.
- *Offset* - An Offset is an accurate shift in the telescope pointing between two Integrations. Integer-pixel Offsets are used for all UKIDSS Integrations, except in the case of Microstepping (see below). At UKIRT, Offsets smaller than $10''$ are fast, so all Offsets used in UKIDSS MSBs are smaller than this. There is a further advantage to using Offsets this small. Because of distortion, an Offset of particular angular size corresponds to a variable size in pixels across the field of view. For Offsets smaller than $10''$ this variation may be neglected, so that Offset frames may be combined without having to rebin the data.
- *Microstep* - A Microstep is a special case of an Offset, where the step in X and Y is on a grid of either $n + 1/2$ or $n + 1/3$ pixels, n being an integer. These two cases are referred to as 2×2 and 3×3 Microstepping hereafter.

Scheme (Survey)	Filter	$t_{\rm exp}$ (s)	μ-step?	Offsets	$t_{\rm tot}$ (s)
1 (LAS, GCS)	ZY	20s	no	2-pt	40
	JHK	5s	2×2	2-pt	40
2 (LAS)	ZY	20s	no	4-pt	80
	JHK	10s	2×2	2-pt	80
3 (GPS)	JH	5s	2×2	4-pt	80
	K	5s	2×2	2-pt	40
4 (DXS)	JK	5s	2×2	25-pt	500
5 (DXS)	JK	10s	2×2	16-pt	640
6 (UDS)	JK	10s	3×3	9-pt	810

Table 4. The different implementation schemes used for the shallow surveys, LAS, GCS & GPS

A variety of Offset patterns are used in the surveys, resulting in three different types of frame in the archive as follows:

- *Normal frames* - A Normal frame corresponds to an Integration.
- *Interleave frames* - A set of Microstepped frames (four or nine, for 2×2 or 3×3 Microstepping, respectively) are interleaved into the sub-pixel grid, to form an Interleave frame (abbreviated 'Leav' elsewhere in this paper and in the WSA).
- *Stack or Interleave-Stack frames* - Where Microstepping has not been used, frames taken at different Offsets are registered, and averaged to form a 'Stack' frame. Where Microstepping has been used, the Interleave frames are registered and averaged to form an Interleave-Stack frame (abbreviated 'Leavstack' elsewhere in this paper and in the WSA).

Note that, because the zero point for a frame relates counts per second to magnitudes, and because averaging is used at all points in combining frames, only $t_{\rm exp}$ is needed to calibrate any frame (rather than the total Integration time, $t_{\rm tot}$).

5.2 Shallow surveys, LAS, GCS, GPS

The choice of $t_{\rm exp}$, whether to Microstep, and the number of Offsets, involves consideration of the relative importance of sampling, overheads, bad pixels, and read-noise relative to sky noise. These reasons motivate the different implementation schemes detailed below. Between them, the three shallow surveys use three different implementation schemes, numbered $1-3$ in Table 4. For each scheme, the table lists successively the scheme number, the filters to which the details apply, the Exposure time, the Microstepping (if used), the number of Offset positions (other than Microsteps) and the total Integration time $t_{\rm tot}$ making up the stacked frame.

5.2.1 LAS implementation

LAS observations are carried out in the filters Y, J, H, and K. The goal is to reach uniform depth in all fields. The MSBs comprise observations of a number of Tiles, and are

Category	Photometric	Seeing	J sky mag/arcsec^2
A	Y	$< 1.0''$	> 15.7
B	Y	$< 1.4''$	> 15.0
C	thin	$< 1.0''$	> 15.7

Table 5. The different categories of observing conditions allowed for LAS observations

of two types, where the filters used are either the pair YJ or the pair HK. If an area has been covered by one pair, every effort is made to cover the same area with the other pair, within a month. Nevertheless, this is not a strict requirement. In order to make the most efficient use of the observing time, a wide range of conditions is used. The choice of MSB to execute depends on whether the conditions fall into one of the three categories listed in Table 5, defined by photometricity, seeing, and J-band sky brightness. Since these are the conditions pertaining at the start of the MSB, the actual conditions may be better or worse. The final criteria which define any data release are set at the QC stage (Section 7).

In 05A, observations were made in the four regions marked LAS1, LAS2, LAS3 and LAS4 in Figure 2. The combinations of filters, implementation strategy (Table 4), and conditions category (Table 5), used for each region are as follows: LAS1 and LAS4 ($YJHK$, 1, A), LAS2 ($YJHK$, 2, B), LAS3 (J, 2, C), which translates as follows: If conditions are photometric, with good seeing, and dark sky, regions LAS1 and 4 are observed, in all filters. If conditions are photometric, but either the seeing is poor, or the sky is bright, or both, Integration times are doubled, and LAS2 is observed, in all filters. If there is thin cirrus but the seeing is good and the sky dark, Integration times are doubled and the first epoch J-band observations in LAS3 are made. Because calibration is made using 2MASS stars in the frames themselves (Section 6.4), the extinction by cloud in these observations is corrected for. Nevertheless the accuracy of the photometry will not be as good as under photometric conditions, and remains to be quantified.

5.2.2 GPS implementation

GPS observations are carried out in the filters J, H, and K, using strategy 3 (Table 4). Depending on conditions, two different types of MSB are executed.

1) In photometric conditions, good seeing $< 0.8''$ at K, and J sky brightness > 15.5 mag/arcsec^2, a single Tile is observed, in filter order J, H then K, providing near-simultaneous observations of the same area.
2) In conditions of thin cirrus, and good seeing $< 0.8''$ at K, first-epoch K-band observations of four Tiles are executed.

5.2.3 GCS implementation

GPS observations are carried out in the filters Z, Y, J, H, and K, using scheme 1 (Table 4), in seeing conditions $< 1.0''$. Depending on the transparency, two different types of MSB are executed.

1) In photometric conditions the full filter set is observed. For J sky brightness > 15.7 mag/arcsec^2, MSBs containing observations in ZYJ may be executed, and for J sky brightness > 15.5 mag/arcsec^2, MSBs containing observations in HK may be executed.
2) In conditions of thin cirrus first-epoch K-band observations are executed.

5.3 Deep surveys

The two deep surveys employ similar strategies. An MSB creates four stack multiframes covering a Tile, in a single filter. Depth is built by repeating the MSB starting from a slightly different base position. For example, for the UDS, the centres are produced with a Gaussian distribution about the global field centre, with a FWHM of $20''$, and truncated at a maximum offset of $2'$.

5.3.1 DXS implementation

DXS observations are carried out in the filters J and K. An MSB comprises observations in one of the filters, of a complete Tile. Implementation scheme 4 (Table 4) was used in 05A, and implementation scheme 5 was used in 05B. The reason for the change to longer Integration times was to reduce overheads. For the EDR, DXS observations required seeing $< 1.1''$, and transparency conditions of thin cirrus or better.

5.3.2 UDS implementation

UDS observations are carried out in the filters J and K. An MSB comprises observations in one of the filters, of the complete UDS Tile. Implementation scheme 6 (Table 4) was used. For the EDR the required observing conditions for J were seeing $< 0.85''$, sky brightness > 16.0 mag/arcsec^2, and for K were seeing $< 0.75''$, with no sky brightness limit. Required transparency was thin cirrus, or better, for all observations.

6 PIPELINE AND CALIBRATION

The WFCAM pipeline is operated by the Cambridge Astronomical Survey Unit (CASU). CASU receives approximately weekly data shipments from UKIRT. Data are stored on LTO tapes, each of the four WFCAM detectors having its own tape and each WFCAM Integration per detector being stored as a single Flexible Image Transport System (FITS) file. Prior to pipeline ingest, the four individual FITS files corresponding to a given Integration are combined into a single multi-extension FITS (MEF) file. This MEF has one header per extension and a primary header describing the data acquisition protocols applicable to the observation necessary to trigger the appropriate pipeline processing components.

We refer the reader to Irwin et al. (2006) for further information on all details contained in this section.

6.1 Pixel data Processing

The pipeline processes data independently on a night-by-night basis. Raw MEFs ingested by the pipeline fall into one of three categories; science frames, flatfields or darks. The first step creates a set of master darks by stacking groups of darks taken at the start of a given night, segregated by Exposure time and read mode. These master darks are then subtracted from all science frames acquired on that night, ensuring dark and science frame Integration times and read modes match. This process removes the reset-anomaly[2] and the dark current, which is very low for the WFCAM detectors.

From here, the data processing strategy is somewhat of a departure from the usual near-IR approach using dark-sky flats which can potentially be corrupted by thermal emission, fringing and large objects. Instead, science frames are flattened by a master calibration twilight flat that is updated at least monthly. The effect of curtaining (see Section 3) on each individual detector frame is then removed with essentially a median filtering algorithm that exploits the 90° rotational symmetry of the quadrants. Following this, a running average median filtered sky correction frame is used for removal of sky structure, scattered light and possible thermal emission in each passband.

Presently, the pipeline makes no correction for persistence, although this is an ongoing issue and a later version may include a module to remove the effect. However, the latest version of the pipeline is able to largely remove cross-talk images. Unfortunately, only WFCAM data acquired in semester 05B, i.e., UDS data and some DXS data, have been processed with this pipeline version. The 05A data, i.e., all LAS, GPS, GCS and some DXS data, were processed with an earlier version that did not correct for cross-talk.

Once frames have been processed up to this point, they undergo a linear flux scaling referred to as a 'gain correction' to bring all detectors to the same average sensitivity level (WFCAM detectors 1 and 4 are respectively the most and least sensitive with a sensitivity ratio of $\sim$ 1.3 in Z, falling to $\sim$ 1.2 in K). If appropriate, the gain-corrected frames are then interleaved to make Leav frames (Section 5.1). Normal and Leav frames are subsequently stacked to make Stacks and Leavstacks. Stacking makes use of a confidence map, derived from the latest flatfield to keep track of pixel sensitivity. Dead pixels and pixels with poor sensitivity, also hot pixels identified from the latest darks are given zero confidence. In the final stage, stacked images undergo source extraction for the production of photometrically and astrometrically calibrated object catalogues.

Note that in addition to Stack and Leavstack frames, for the DXS and UDS, a set of deep stacks have been generated, using data across all nights covered by the EDR in certain Tiles (see Section 8). Catalogues are also generated from these deep stacks.

[2] The reset anomaly is a ramp-like additive component caused by the capacitive behaviour of the detector following a reset and the variation in time, as a function of a given pixel's position, after which the first read for that pixel is made

6.2 Catalogues

A source extraction routine based on the methodology of Irwin (1985) is run on the pipeline processed stacked images. Source detection searches for groups of 4 or more connected pixels that all lie above a threshold of 1.5 times (1.25 times for frames interleaved to 0.2"/pixel or 0.133"/pixel) the local background sky noise. A global background following algorithm (Irwin & Trimble 1984) is used to track varying background over each stacked frame on a scale size of 25.6" (64 WFCAM pixels). This scale is a compromise between being small enough to accurately follow rapidly varying background and large enough to sample a sufficient unobscured area of sky. The initial background value in each 25.6"×25.6" block is derived using a robust iterative k-sigma clipped median estimator. The resulting array of block values are then further filtered to remove outliers due to, for example, bright stars, and this coarse grid is bilinearly interpolated back to the original pixel resolution. Pixels flagged in the confidence map as having zero weight or having null pixel values in the image are ignored during the background estimation phase.

The confidence map is used to weight pixels during image detection. The current version of the pipeline does not make use of this weight information in deriving object parameters. For each detected object, a series of apertures over a range of radii are overlaid on the object and the background-corrected flux summed within the aperture. These fluxes form the sequence of fluxes '`aperFlux`N' stored in the WSA where $N = 1$ to 13 (see Section 9). Apertures are 'soft-edged' in the sense that flux in pixels dissected by the aperture boundary is scaled according to the fraction of pixel enclosed by the boundary. This compensates for aperture edge effects.

All detected objects are deblended, the `aperFlux` quantities being corrected to remove flux contribution from any neighbouring sources and so that they give a measure of the total flux. The aperture correction is computed from the image seeing under the assumption that the sources are point-like. Flux errors are computed from photon statistics, the read-noise and background error. The pipeline outputs object catalogues as binary MEF tables which are directly ingested by the WSA. A variety of quality control parameters, such as stellar ellipticity, seeing, sky brightness, zero point and extinction (see below for these latter two) are output by the pipeline and written into the MEF tables. Currently, PSF and Sersic profile fitted photometry is not supported by the pipeline, but will be in a future release.

6.3 Astrometric calibration

Catalogue object co-ordinates are first corrected for WFCAM's non-uniform pixel scale across the field of view. This takes the form of the radial distortion

$$r_{\rm true} = r + kr^3 \qquad (1)$$

where $r_{\rm true}$ is the true on-sky angular distance from the optical axis and r is the distance measured from a WFCAM image. For WFCAM, the constant k is $\sim -50/\mathrm{radian}^2$, depending on the filter (e.g., in H, k is around $-50/\mathrm{radian}^2$ and in K around $-53/\mathrm{radian}^2$). WFCAM commissioning data clearly showed that astrometric systematics were al-

ready below the specified requirement of $< 0.1''$ without the need to include distortion terms of r^5 and higher.

With the radial distortion removed, astrometric calibration is provided by the Two Micron All Sky Survey (2MASS; Cutri et al. 2003). Using the 2MASS point source catalogue, the final astrometric solution is obtained by solving the following linear transformation for all objects in each stacked detector frame;

$$x' = \mathrm{a}x + \mathrm{b}y + \mathrm{c} \quad ; \quad y' = \mathrm{d}x + \mathrm{e}y + \mathrm{d}, \tag{2}$$

to allow for translation, scaling, rotation and shear. Since 2MASS astrometry is based on Tycho 2 and is in the International Celestial Reference System (ICRS), so too is WFCAM astrometry. This does not require an Equinox to be specified and for most practical purposes, this is (almost) equivalent to Equinox 2000 in FK5[3]. Once computed, the astrometric solution is written into the catalogue MEFs and back-propagated to the stacked and component image MEFs.

6.4 Photometric calibration

All WFCAM data processed by the pipeline are calibrated into the Vega system, using 2MASS stars as calibrators, but with photometry converted into the WFCAM filter system (see Hewett et al. 2006, for details of the WFCAM filters). The motivation for basing the calibration on 2MASS is:

- The 2MASS global calibration is accurate to better than 2% across the entire sky (Nikolaev et al. 2000).
- There is always an abundance of 2MASS stars in each WFCAM Observation that are not saturated (typically 60-1000, depending on Galactic latitude).
- Measuring the calibrators at exactly the same time as the targets enables photometric calibration even during non-photometric conditions (limited by the uniformity of the cloud cover).

However, the WFCAM observing strategy dictates the measurement of UKIRT faint standards throughout each night to ensure that a calibration independent from 2MASS can be derived should the need arise.

The first step in the procedure for converting measured fluxes to magnitudes is to identify 2MASS Point Source Catalogue stars (with error $\sigma_m(\mathrm{2MASS}) \leqslant 0.1$) in each stacked detector frame. The photometry for each 2MASS source is transformed into the WFCAM $ZYJHK$ system using the following empirically derived colour terms:

$$\begin{aligned}
Z_{\mathrm{WFCAM}} &= J_{\mathrm{2MASS}} + 0.95 * (J_{\mathrm{2MASS}} - H_{\mathrm{2MASS}}) \\
Y_{\mathrm{WFCAM}} &= J_{\mathrm{2MASS}} + 0.5 * (J_{\mathrm{2MASS}} - H_{\mathrm{2MASS}}) \\
J_{\mathrm{WFCAM}} &= J_{\mathrm{2MASS}} - 0.075 * (J_{\mathrm{2MASS}} - H_{\mathrm{2MASS}}) \\
H_{\mathrm{WFCAM}} &= H_{\mathrm{2MASS}} + 0.04 * (J_{\mathrm{2MASS}} - H_{\mathrm{2MASS}}) - 0.04 \\
K_{\mathrm{WFCAM}} &= K_{\mathrm{2MASS}} - 0.015 * (J_{\mathrm{2MASS}} - K_{\mathrm{2MASS}})
\end{aligned}$$

The 2MASS calibrators are then matched to WFCAM sources in the frame. Using $1''$ radius aperture-corrected fluxes for the WFCAM sources, a per-star zero point is calculated as

$$ZP_i = m_i(\mathrm{2MASS}) + 2.5\log10(\mathrm{N_i}/\mathrm{t_{exp}}) \tag{3}$$

where N_i is the counts in ADU of source i, corrected to account for the variable pixel scale noted above, and t_{exp} is the Exposure time in seconds. A further extinction correction is applied, using a default extinction of 0.05 mag per unit airmass, assumed for all nights and all filters.

The photometric zeropoint for a given stacked detector frame is then simply the median zeropoint over all unsaturated stars. Detector-to-detector differences in the zeropoint are largely removed by the gain correction applied during pixel data processing and residuals are measured to be $\leqslant$ 1%. A typical WFCAM Observation contains in the range of 60-1000 2MASS calibrators in total over the four detectors, dependent on Galactic latitude, with a median of around 150 unsaturated 2MASS stars with $\sigma_{JHK}(2MASS) \leqslant 0.1$. 2MASS is therefore expected to calibrate the WFCAM data to $\sim$ 1%. Of course, the calibration will be limited by the global systematics in 2MASS (see Nikolaev et al. 2000), the accuracy and robustness of the transformations between the filter systems (in particular, the WFCAM J-band filter is somewhat narrower and redder than the 2MASS J-band filter), and by the fact that the respective observatories are at significantly different altitudes.

The photometric accuracy of the EDR data is quantified in Section 7.

7 DATA QUALITY CONTROL

All products in the EDR have passed through a series of QC tests to filter out sub-standard and corrupt data. Sub-standard data do not meet the requirements specified by a given survey or project, generally due to unacceptable observing conditions, WFCAM peculiarities or poor pipeline processing. Corrupt data can occur for a variety of technical reasons, most commonly at the data acquisition stage.

The SV process identified a variety of idiosyncrasies giving rise to sub-standard data. These were largely corrected during the early stages of surveying and processing. However, a small number have proven impossible to correct on a short timescale (e.g. moon ghosts and bad detector channels; see Section 7.2). Our quality control procedure, like the WFCAM pipeline and WSA, is presently under continued development. As such, although most of the data in the EDR are near final survey quality, users must be aware that some would most likely fail a more stringent and thorough filtering process.

The purpose of this section is threefold. Firstly, we detail the QC checks that the EDR data were passed through and quantify the amount of data rejected. Secondly, we highlight some of the peculiarities that can arise in WFCAM data to alert users to the possibility of what may, to a small degree, have passed through the QC. Thirdly, we provide various measures of the quality of the data that have been deemed suitable for inclusion in the EDR.

7.1 QC procedure

The checks that constitute the QC procedure fall into two categories; those that validate the architecture of the data and those that verify its quality. The architectural tests are

[3] MEFs have the FITS keyword RADECSYS = 'ICRS' set. For backwards compatibility with existing software, EQUINOX = 2000.0 is left as is.

carried out before testing quality and can be divided into two:

- *Data composition* checks ensure that all data components are present in the archive as expected, i.e., that all stacked frames have associated catalogues, all image MEFs have data in all four detectors, frame types are correct (e.g. twilight flats should not masquerade as science frames) and that all file complements are as expected, per filter, per project, per survey, (e.g. each Y-band Observation in LAS1 must have 2 Normal frames, 1 Stack & 1 Stack confidence map – 'Stackconf').
- *Attribute integrity* checks ensure that no indefinite, default or (where applicable) null values are present in certain key attributes. In addition, checks are performed to verify that catalogues have the correct epoch data (e.g., LAS should not have any `j_2` attributes yet).

Once data are architecturally verified, they are subjected to the quality checks. This is an iterative process, each stage refining the data by imposing tolerances on a range of quantities. Since the data in the current release are mostly from semester 05A when the alignment and therefore image quality of WFCAM was not optimal, we have relaxed these tolerances to a degree.

Firstly, data are rejected based on the QC parameters that are written into the MEF headers by the WFCAM pipeline (see Section 6.2). These parameters are the seeing, sky brightness, photometric zero point and average stellar ellipticity, all of which apply to individual detector frames (via the WSA attributes `seeing`, `skyLevel`, `PhotZPCat` & `avStellarEll` in table `MultiframeDetector`). Secondly, limits are placed on the derived quantities, depth, as given by equation (4), and the total number of objects catalogued per detector. Generally, data tolerances are survey-specific. We will refrain from providing an exhaustive list of the exact range of allowed parameter values per survey per filter, although two global tolerances can be easily quantified; all detector frames having an average stellar ellipticity of > 0.25 or $5\times$ the average survey object number density were rejected.

In addition, the internal astrometric and photometric accuracy are derived by computing the standard deviation and mean of the distribution of differences in magnitude and position between duplicate objects extracted from overlap regions. Any outliers are traced to individual detector frames where photometric or astrometric calibration has gone wrong, and those data rejected.

Finally, all stacked frames are visually inspected. The philosophy here is to provide a final safety net to catch bad data where the QC tests fail. Frames are checked to identify problems that manifest themselves cosmetically, such as poor flatfielding, moon ghosts, poor sky/thermal emission correction and poor dark correction. These mostly fall under the remit of data flaws, discussed in Section 7.2.

Data can be rejected at the multiframe or the detector level, depending on the reason for failure. Some multiframes therefore have less than four associated detector frames. All rejections are back-propagated, removing stacked data constructed from rejected normal data, catalogues without pixel data (and vice versa), and multiframes with four independently rejected detector frames.

The quantity of data rejected by the QC procedure over the whole of the EDR (i.e. the EDR+ database) as a fraction of each survey are as follows: LAS 4.3%, GPS 14.4%, GCS 2.4%, DXS 1.9% & UDS 0.0%.

7.2 Data flaws

Whilst visual inspection of the stacked frames has identified and removed all stacks that contain obvious flaws, visual inspection of all ∼90,000 normal frames in the EDR is not feasible. This section therefore illustrates typical flaws that can arise in the data so that users are aware of their possible presence.

Figure 3 again shows the layout of the four WFCAM detectors, and provides illustrations of some of the artifacts that can occur in images. These are considered in turn below. A number of these effects give rise to false detections in any frame with the consequence that the catalogues contain a number of entries for objects that have apparently interesting colours, but are not real.

Channel bias Offsets

In a few percent of frames the counts in any channel may be offset high or low, by a few counts, or more rarely by tens of counts. Because of the lower sky counts the effect is more often visible in the shorter wavelength bands Z, Y, and J. Two channels in array 4, marked 'C' in the figure are particularly prone to this variable bias level. The offset can vary from one frame to the next, and therefore is not effectively removed by subtraction of a dark frame. Very occasionally all the channels in an array are afflicted, such that the entire channel pattern is visible, as in the case of array 4 in the illustration.

Channel bias offsets are particularly troublesome in interlaced data, since every fourth pixel (or ninth in 3×3 Microstepping) is offset in level, resulting in a 'bed-of-nails' pattern. In the worst cases, the bias offsets confuse the object detection algorithm, resulting in a large number of spurious sources in the channel. We have attempted to identify the worst cases and removed the frame and catalogues from the release database. Both hardware and software solutions to the problem of channel bias offsets are being pursued.

Images of stains on the field lens

Because the field lens (Section 3) is located close to an intermediate focus, stains or dust on the lens, radiating thermally or scattering moonlight, are visible in some frames. The three worst examples are marked 'L' in Figure 3, but there are numerous other smaller ring features. When the illumination is fairly constant these spurious images are successfully removed by the pipeline, at the stage of sky subtraction. However, the problem is more difficult to treat if the intensity is variable, for example as the moon transits into or out of the dome slit.

Persistence images

Persistence is an issue for saturated stars. The level of persistence is a function of source count rate, wavelength (i.e., filter), and number of reset/reads, and can be visible over several frames. Persistence images are characteristically

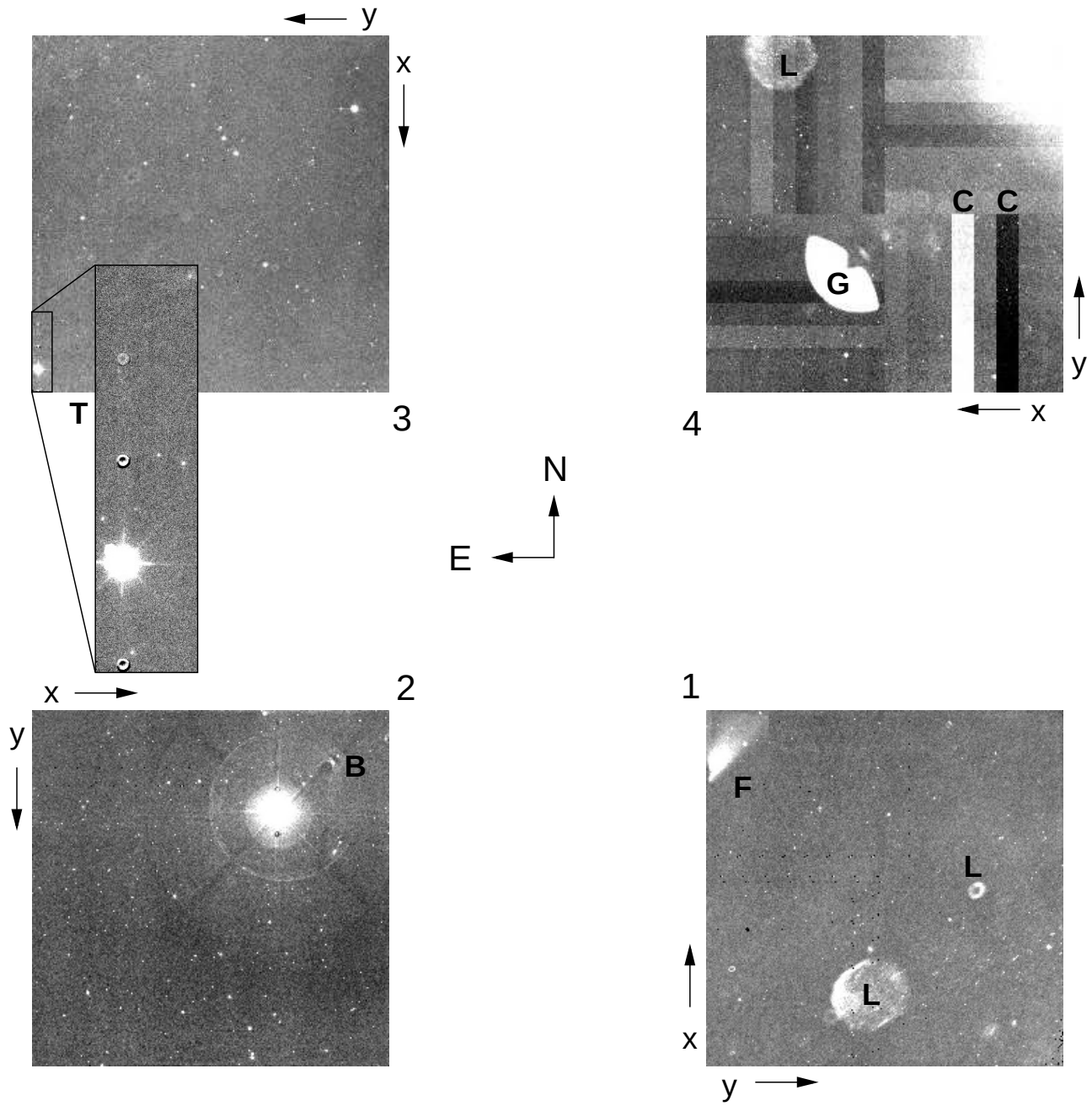

Figure 3. WFCAM focal plane showing composite of various data artifacts that can arise in WFCAM data, described in detail in the text. North is up and East to the left as marked. Data artifacts key: C - the two worst channels with variable bias level, L - images caused by dirt on the field lens, F - flare persistence image that appears after filter changes, B - 'bow-tie' feature in the halos of bright stars, G - bright ghost from moonlight shining on the field lens, T - cross-talk image sequence associated with bright star.

the size of the saturated part of their progenitor image. Images persisting across a number of frame will follow any Offset pattern employed, and in such cases the effect usually stacks out.

The flare image marked 'F', is also a result of persistence, and is often visible in 05A data in the first frame taken after a filter change (because the array has been exposed to unfiltered light (Section 3), and consequently saturated). For the 05B data a short sequence of dark frames following each filter change was implemented, to flush persistence images, and the flare image should be absent.

Bright moon ghosts

In some circumstances, apparently when the moon is shining directly onto the field lens, bright ghost images occur, such as the image marked 'G' in array 4 in Figure 3. We believe that the appearance of the ghosts depends on the angle of inclination of the moon relative to the optical axis. At large angles highly elongated arcs appear. The exact cause of these images is under investigation. It is possible that the ghosts arise from reflection off the mounting arrangement of the autoguider auxiliary lens, at the centre of the field lens.

We have attempted to identify all the brightest examples of moon ghosts, and remove the affected frames, and accompanying image catalogues. Moon ghosts occur both in 05A and 05B data. For the next WFCAM campaign a baffle extending above the field lens should reduce the problem. Once the cause has been identified it will be possible to avoid the problem by appropriate scheduling of the observations.

Cross-talk images

The zoom image in Figure 3 of a portion of array 3 illustrates the problem of cross talk. Here, a sequence of spurious images can be seen. These are caused by the bright star, appearing in some or all of the 7 other channels of the quadrant in which the star is located. The images are always offset across the channel width by an integer multiple of 128 pixels (256 or 384 pixels for 2×2 or 3×3 Microstepping respectively). Cross-talk images in adjacent channels have features at $\sim 1\%$ of the differential flux of the source, dropping to lower levels further from the source, but sometimes extending across the entire quadrant. The appearance of the cross talk images depends on the counts in the star, and, for bright stars the shape matches the spatial derivative of the profile of the star. Therefore for bright unsaturated stars the cross-talk images have a half-moon appearance, while for saturated stars, where the counts at the centre of the image are constant at the saturation value, the cross-talk images have the curious washer appearance shown.

Cross-talk images are particularly pernicious because they appear in the same location relative to the bright star, for different filters. Therefore the detections are matched across bands, and the objects appear in the catalogues as entries with peculiar colours.

Diffraction pattern for bright stars

The image of a bright star in array 2 is shown in Figure 3. The diffraction pattern shows 8 spikes, from two spiders, one supporting the secondary, and the other the guider auxiliary lens, above the field lens. The spikes can extend to large angles, $\sim 20'$ and therefore may be visible in some frames, where the bright star itself is not visible. There is a low-level feature in the point spread function, marked 'B' in Figure 3, which has the shape of two bow ties. Similarly these can be visible in some frames, where the star itself is outside the field of view.

7.3 Data quality

In this section, we quantify the quality of data in the EDR. Specifically, we consider the accuracy of the photometric and astrometric calibration, image quality (i.e., seeing and stellar ellipticity), variation of zero points and depths reached by the different surveys.

7.3.1 Photometric calibration

Internal photometric accuracy

As a first test of the photometry, we consider the photometric consistency of duplicate objects in overlapping edges of detector frames that arise from constructing Tiles. Figure 4 shows the median difference in magnitude of duplicate objects in each filter in the LAS and GCS, binned by J magnitude. The standard deviation of the differences in each bin are shown by the error bars. As one would expect, the error bars increase in size with increasing J-band magnitude. There is remarkably little variation between filters. The size of the error bars is consistent with the accuracy of the external photometric calibration as seen in Figure 5.

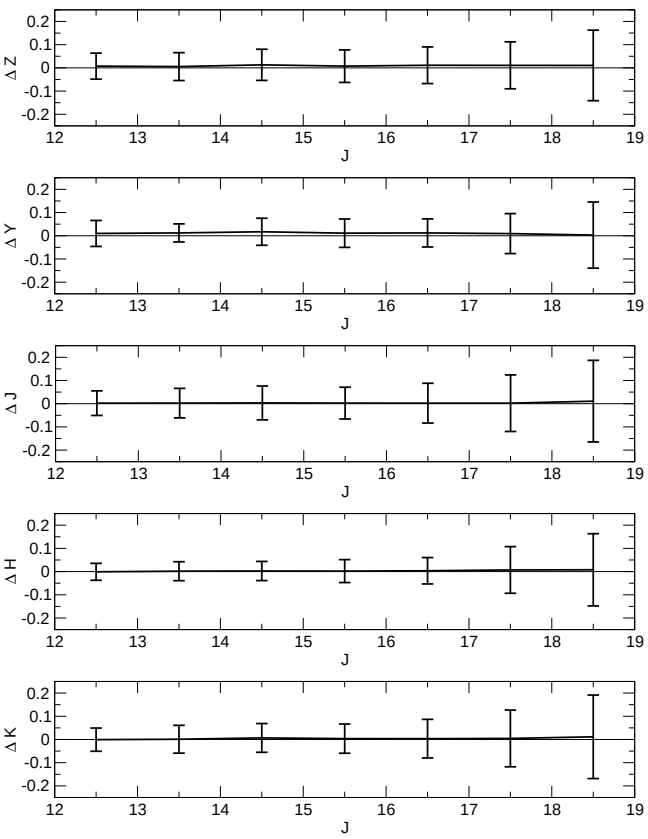

Figure 4. Photometric consistency of duplicate objects found in overlapping detector frame edges in LAS and GCS. Plotted is the median difference in magnitude between duplicates binned by J magnitude. Error bars are the standard deviation of the differences in each J bin.

External photometric accuracy

Photometric calibration is discussed in Section 6.2. Since there is a median of around 150 unsaturated 2MASS stars with $\sigma_{JHK}(2MASS) \leqslant 0.1$ over the four detectors in a WFCAM Observation, 2MASS is expected to calibrate the WFCAM data to $\sim 1\%$. However, this is limited by systematics in 2MASS and the accuracy of the 2MASS-WFCAM colour transformations.

To quantify this, we have analysed J, H and K photometry for a total of 600 measurements of 46 fiducial stars (drawn from the UKIRT faint standards, Hawarden et al. 2001) measured on 19 photometric nights. We find that the RMS scatter for these measurements is less than 2%, meeting the UKIDSS requirement for photometric accuracy (see Hodgkin et al. 2006). The quality of the Z, Y and narrowband-filter calibration has not yet been quantified.

Figure 5 shows a scatter plot of the difference between the WFCAM calibrated magnitudes and UKIRT Fast-Track

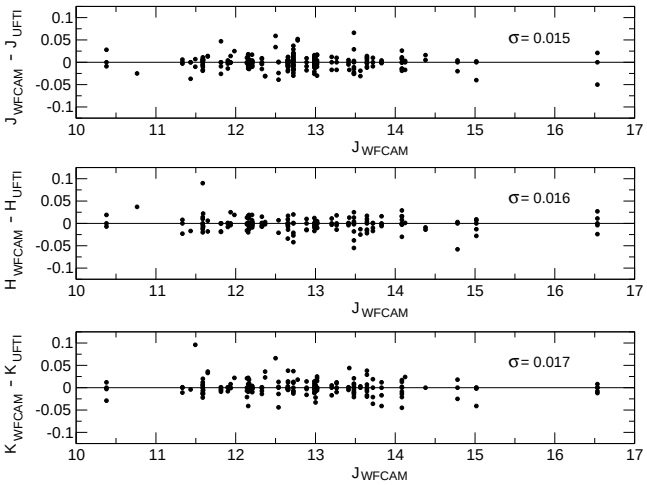

Figure 5. Difference between 2MASS calibrated WFCAM magnitudes and UFTI magnitudes of 46 UKIRT faint standard stars in J, H & K as a function of WFCAM J magnitude.

Imager (UFTI) magnitudes for the 46 UKIRT faint standard stars in J, H & K. The standard deviation for each filter is displayed on the plot and shows that data can be calibrated to $< 2\%$.

7.3.2 Astrometric calibration

Internal astrometric accuracy

In the same spirit as the internal photometric consistency measurements, we have measured the astrometric consistency of duplicated objects in overlapping edges of detector frames.

Figure 6 shows the variation of the median and standard deviation of the difference in RA and Dec of duplicated objects, as a function of binned J-band magnitude and Galactic latitude. The plots show that there is no systematic offset in the median of the differences, nor a noticeable increase in their scatter at higher Galactic latitudes (where there are considerably fewer stars to provide the astrometric solution) or fainter J magnitudes.

External astrometric accuracy

After correcting catalogues for the radial distortion given by equation (1) and after applying the linear transformation given by equation (2), the residuals between positions of identified 2MASS stars and positions from the 2MASS point source catalogue have an average RMS of $\sim 0.1''$.

We demonstrate this by stacking WFCAM-transformed positions of 2MASS stars from ∼1100 Observations acquired within a week's worth of EDR data. Selecting all 2MASS stars with a photometric signal-to-noise ratio of > 10 in all of J, H and K, to ensure that 2MASS astrometry errors are $\lesssim 0.1''$, yields ∼150,000 stars per detector. Figure 7 shows the average offset between 2MASS and WFCAM astrometry in spatial bins across the WFCAM detectors. The median RA and Dec in this plot is -0.001" and 0.002" respectively. The standard deviation of the RA and Dec residuals is 0.087" and 0.080" respectively.

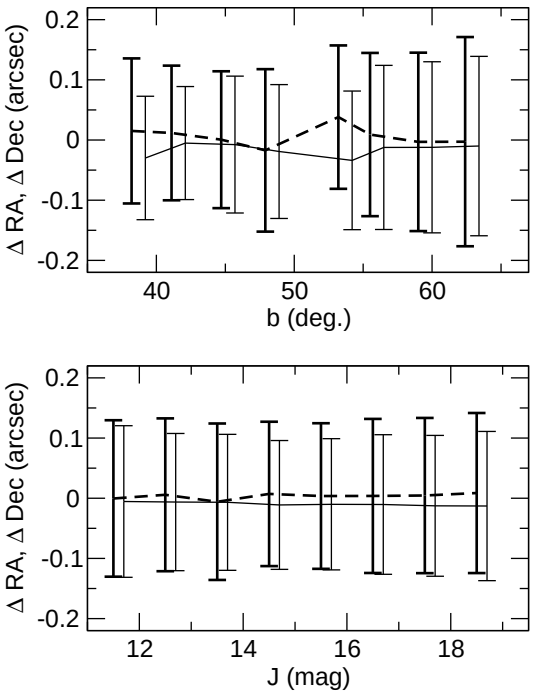

Figure 6. Astrometric consistency of duplicate objects found in overlapping detector frame edges in LAS. *Top*: Median difference in RA (thick, dashed) and Dec (thin, solid) between duplicates binned by Galactic latitude. *Bottom*: Same as top but plotted against binned J magnitude. Error bars are the standard deviation of the differences in each bin. Dec points are offset from RA points for clarity.

Filter	all	$< 1''$
Y	20.23	20.25
J	19.52	18.51
H	18.73	18.79
K	18.06	18.12

Table 6. LAS 5σ median point source sensitivity by filter in the EDR database. The two columns are for all seeing and just those data with seeing $< 1''$.

7.3.3 Shallow survey data characteristics

Figures 8 and 9 show scatter plots of depth, as given by equation (4), versus seeing, stellar ellipticity, zero-point and sky brightness for data in the LAS and GCS EDR database. Due to source crowding and nebulosity in the GPS data, the pipeline derived catalogue properties can generally not be trusted, hence we omit the GPS in this case. However, since all data are processed in the same way and since the implementation of the GPS observations are very similar to those of the LAS and GCS, we expect the GPS to be no different from the LAS and GCS in terms of these properties.

Tables 6 and 7 show the 5σ median point source sensitivity of EDR data by filter for the LAS and GCS respectively. The tables give the median depth for LAS and GCS data in the EDR database, both for all seeing and for data with seeing better than $1''$, the latter being representative of what we expect from survey-quality data in forthcoming releases.

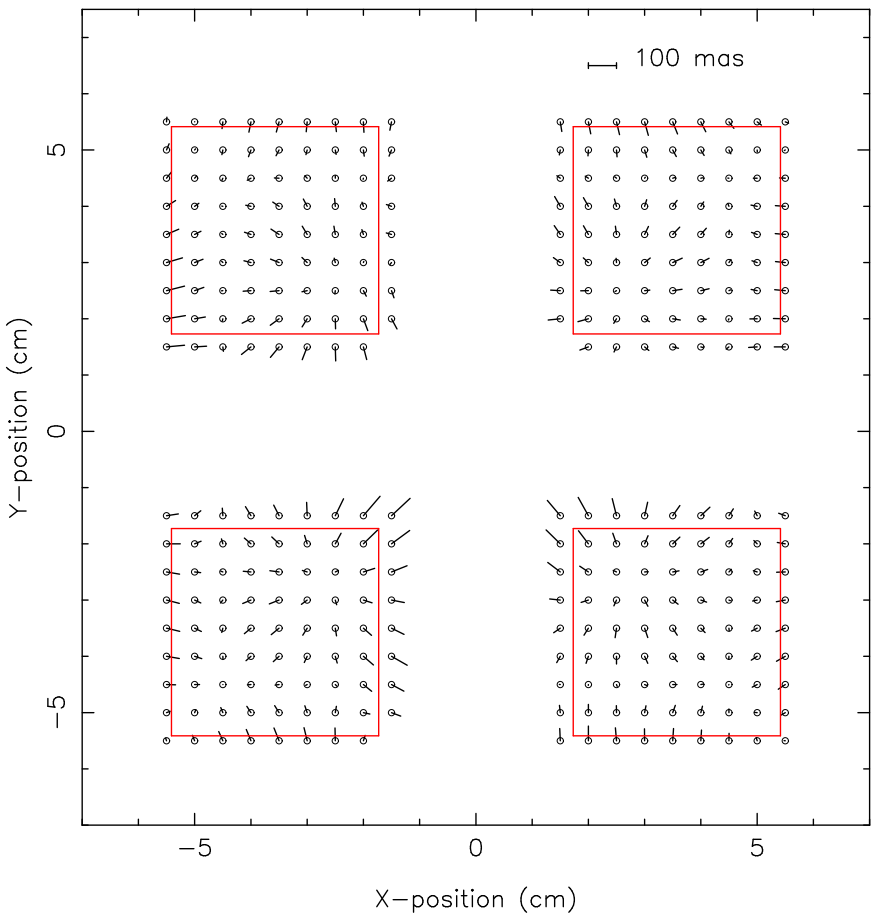

Figure 7. Distribution of astrometric error across WFCAM's field of view calculated by stacking the positions of ∼150,000 2MASS stars per detector from a week's data.

Filter	all	$< 1''$
Z	20.29	20.40
Y	19.92	20.05
J	19.40	19.46
H	18.79	18.80
K	18.12	18.12

Table 7. GCS 5σ median point source sensitivity by filter in the EDR database. The two columns are for all seeing and just those data with seeing $< 1''$.

7.3.4 Deep survey data characteristics

Figure 10 shows how depth in the DXS and UDS stacked frames varies with total Integration time in J and K. Fitting the form $a + 2.5 \log 10(t^b_{\rm exp})$ for depth gives $b = 0.494$ for J and $b = 0.503$ for K, demonstrating that the depth of the deep surveys is scaling as expected.

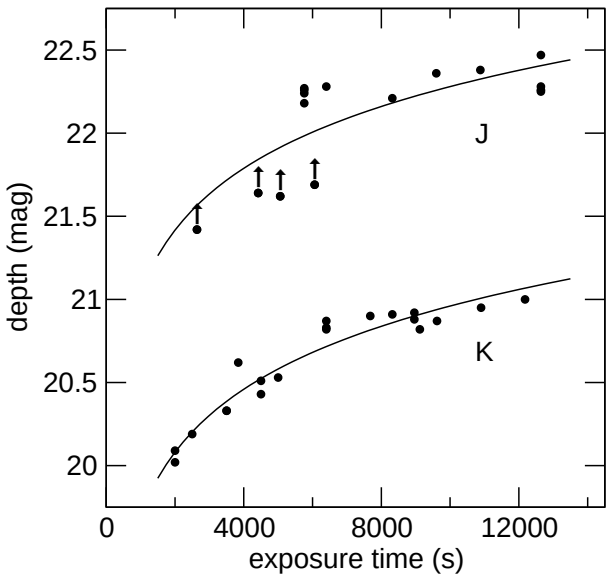

Figure 10. Variation of depth reached as a function of total Exposure time in stacked deep survey (DXS & UDS) data. The four points with arrows are lower limits due to the stacking issue discussed in Section 8.2.

8 THE CONTENTS OF THE EDR

Pipeline processed images and catalogues are stored in and accessed via the WSA (Section 9). As described in Sections 6 and 5.1, the pipeline stacks all Normal and Leav science frames. Only frames from the same MSB executed on the

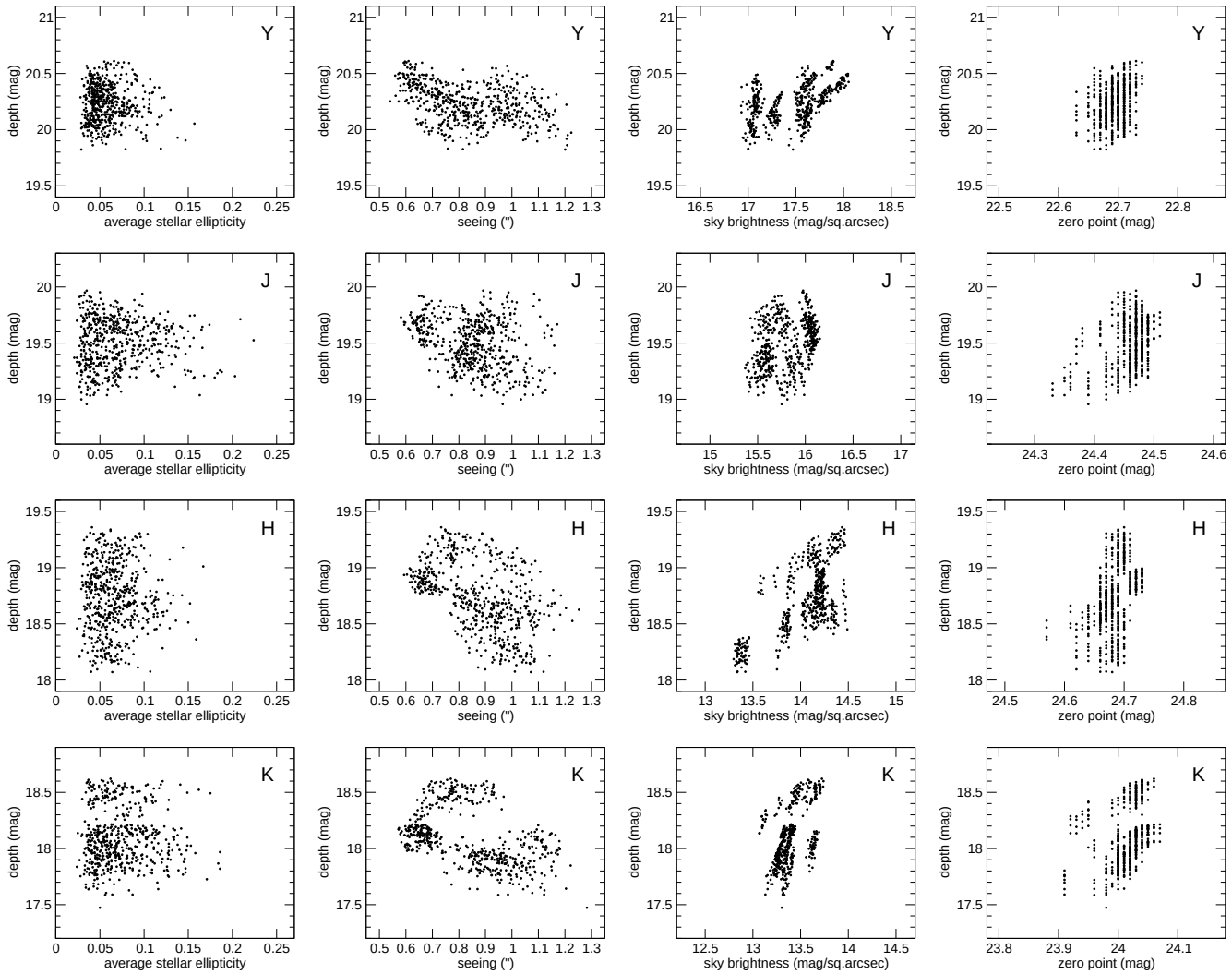

Figure 8. LAS data quality, plotting depth from equation (4) versus average stellar ellipticity, seeing, sky brightness and zero point in Y, J, H & K. Each point represents one detector frame in the EDR database.

same night are stacked by the pipeline, generating Stack or Leavstack frames.

All five UKIDSS surveys have associated Stack and/or Leavstack frames which all have corresponding catalogues. In the three shallow surveys, Stack and Leavstack frames are the deepest stacked data that exist. However, in the DXS and UDS, an extra set of deep stacks are provided, where all data with coincident base positions across all nights are stacked. These deep stacks also have associated source catalogues.

In this section, we divide the description of the EDR data contents into that of the shallow surveys and that of the deep surveys.

8.1 Shallow survey data

LAS, GPS and GCS data in the EDR were observed exclusively in semester 05A, between the dates 15th May 2005 to 31st July 2005. The data include Stack & Leavstack frames, with their associated catalogues, and Normal & Leav frames.

Survey	Z	Y	J	H	K	EDR
LAS	-	33.5	89.4	57.3	51.0	27.3
GPS	-	-	16.8	17.8	57.9	14.9
GCS	13.4	14.4	16.0	32.1	29.7	7.0

Table 8. Coverage of the shallow surveys (deg^2) in the EDR+ database, broken down by filter. Last column lists coverage in the EDR database.

Table 8 shows the coverage of each survey in the EDR and EDR+ databases by filter.

In the LAS, data in the EDR database exist in projects LAS2 (the north-eastern most corner of the equatorial block) and LAS4 (the eastern half of the Millennium Galaxy Catalogue, MGC, Liske et al. 2003). In addition to these, the EDR+ database contains data in projects LAS1 (Virgo) and LAS3 (eastern most quarter of the northern block). LAS3 contains only J band data, the purpose of this project being to acquire data early on for proper motion studies and to enhance the allocation of time to the LAS by allowing ob-

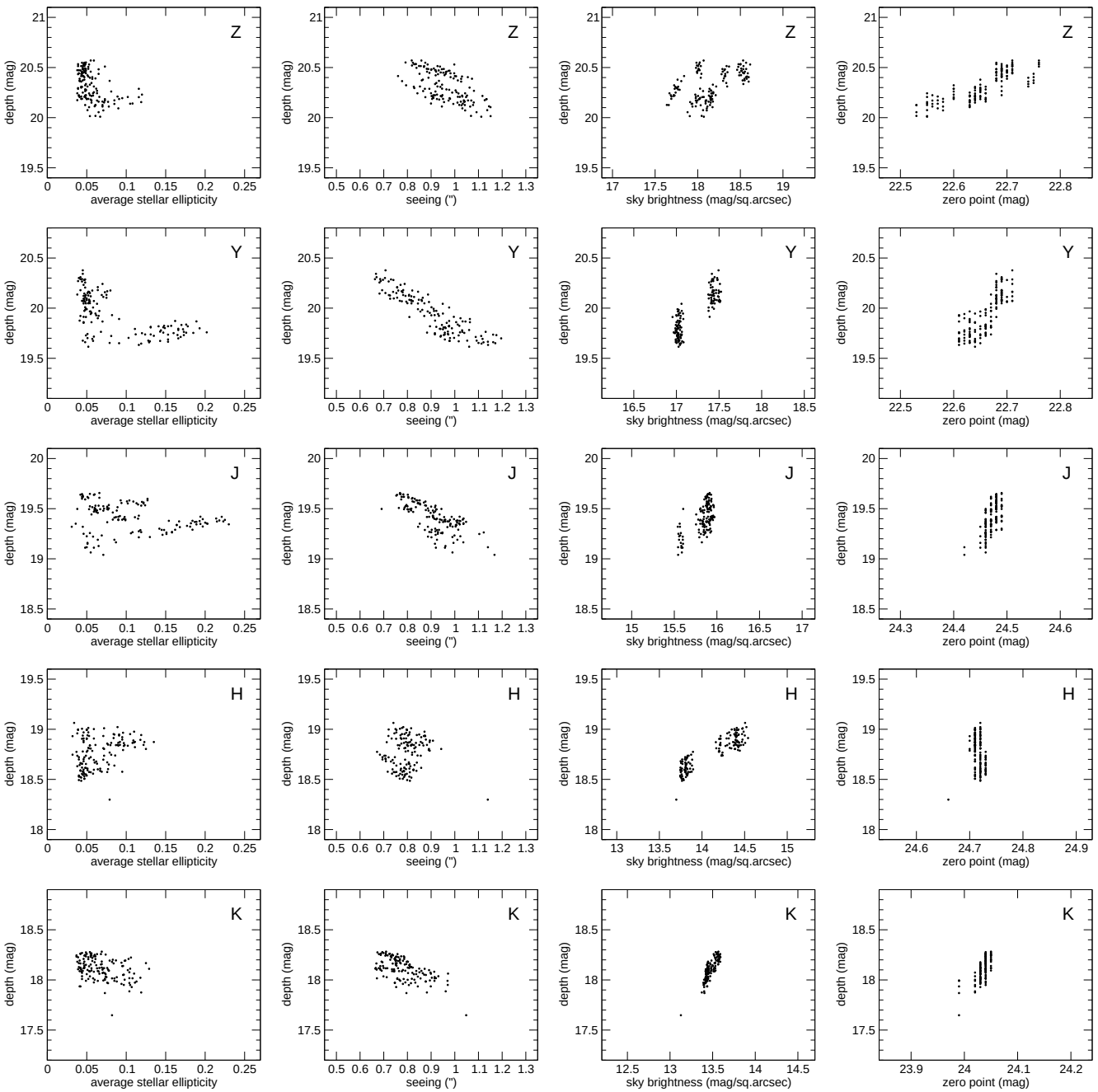

Figure 9. GCS data quality, plotting depth from equation (4) versus average stellar ellipticity, seeing, sky brightness and zero point in Z, Y, J, H & K. Each point represents one detector frame in the EDR database.

serving in thin cirrus. Figures 11 and 12 show data coverage in the four LAS projects. Dark and light grey tiling shows the total coverage (EDR+ database) with dark tiling specifically indicating EDR database coverage. The total LAS coverage is 27.3 deg^2 in the EDR database and 114.2 deg^2 in the EDR+ database.

GPS data in the EDR+ database are limited to the $-2^\circ < \mathrm{l} < 107^\circ$ block. Within this, EDR database coverage is specifically limited to $|\mathrm{b}| < 1$, $-2 < \mathrm{l} < 107$ and $|\mathrm{b}| < 5$, $30 < \mathrm{l} < 45$. Figure 13 shows the data coverage. In total, the GPS data cover 14.9 deg^2 and 59.7 deg^2 in the EDR and EDR+ databases respectively.

Finally, for the GCS, the EDR database holds data for the open cluster Sco. EDR+ database coverage additionally includes 1.75 Tiles in the star forming association Coma-Ber. Figure 14 shows the data coverage. The GCS covers a total area of 7 deg^2 and 38.3 deg^2 in the EDR and EDR+ databases respectively.

8.2 Deep survey data

For the DXS and UDS data, there is no distinction between the EDR and EDR+. DXS data span semesters 05A and 05B between the dates 9th April 2005 and 28th September

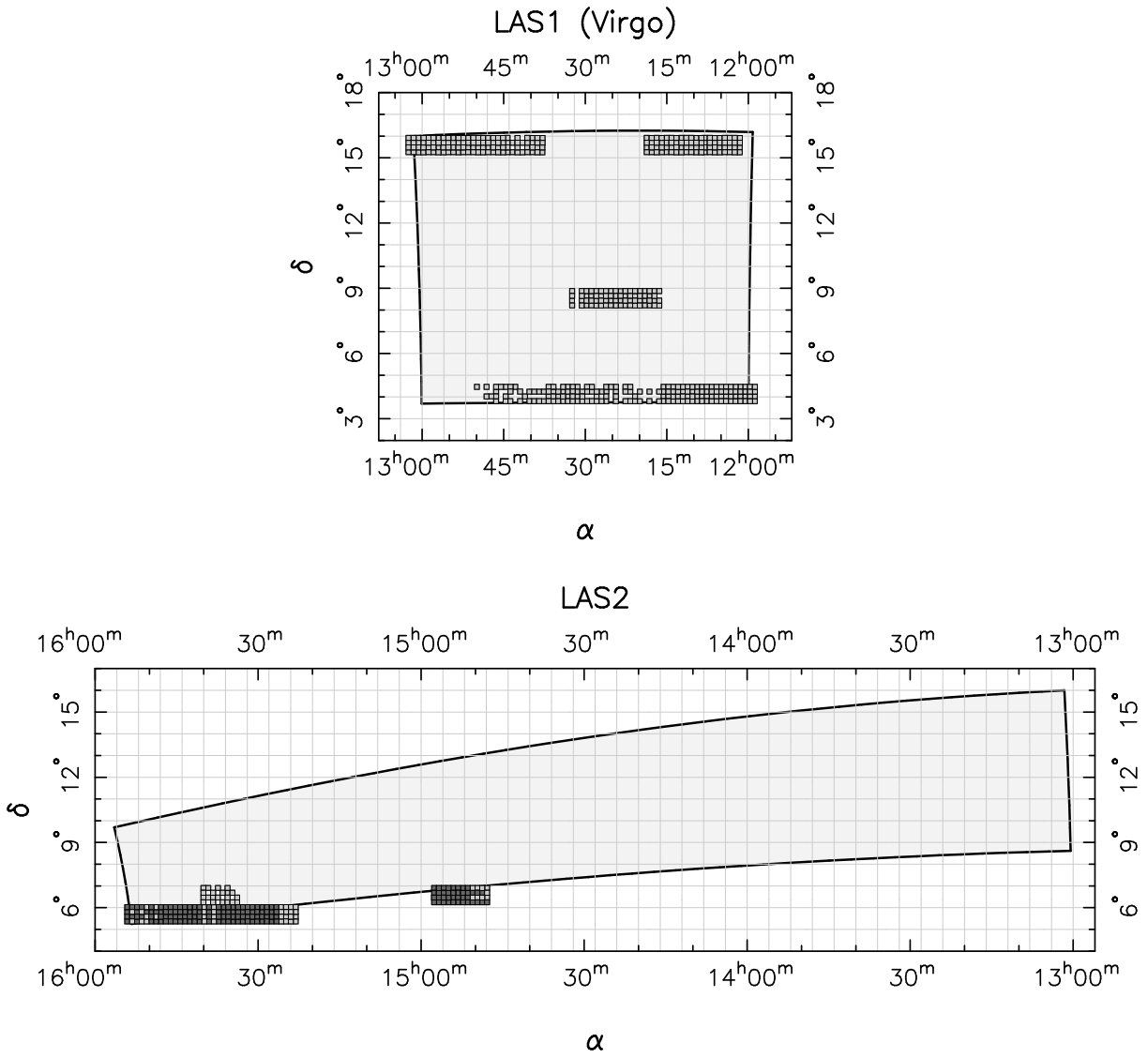

Figure 11. LAS data coverage in the EDR database (all of $YJHK$; dark grey tiles only) and the EDR+ database (light and dark tiles) for projects LAS1 and LAS2. Each small square is a detector frame.

2005. UDS data are from semester 05B only, from the 12th to the 28th September 2005.

Adhering to the data architecture of the shallow surveys, the DXS and UDS data comprise Normal, Leav and Leavstack frames. Leavstack frames are the same stacks present in the shallow survey data. DXS Leavstacks are interleaved at the scale of 0.2"/pix and UDS Leavstacks at the scale 0.133"/pix. The J and K coverage of the DXS Leavstacks is shown in Figures 15 and 16. Figure 17 also gives a graphical representation of the DXS coverage by plotting the area that attains a given minimum depth as a function of that minimum depth. We have not shown UDS coverage since all J and K data lie in one Tile, hence we simply quote depths (Table 10).

In addition to the Leavstack frames, the DXS and UDS data include deep stacks created by stacking all coincident Leavstack frames across all nights. For the DXS, deep stacks were created with the same stacking algorithm used by the WFCAM pipeline. Only sufficiently deep Tiles were stacked in this way and these are labelled in Figures 15 and 16. In the WSA, the DXS deep stacks are referred to as 'Deepleavstack' frames and are the usual multiframes holding 4 detector frames.

For the UDS, deep stacks were created from QC'd Leavstack frames using TERAPIX's SWarp package (Bertin et al. 2002) with a lanczos3 kernel. Unlike the DXS deep stacks, UDS Leavstacks were mosaiced together to make a Tile. Since the UDS data are Microstepped to 1/3 of a WFCAM pixel, the final J and K interleaved and stacked Tiles are $\sim 24000 \times 24000$ pixels, occupying some 3 Gb each on disk. To ease handling, these have been divided into four quarters. In the WSA, these quarters are referred to as 'Mosaicdeepleavstack' frames. Unlike all other stacked data in the WSA, astrometry of the deep UDS stacks uses tangential projection (TAN) rather than the usual zenith polynomial projection (ZPN).

Both DXS and UDS deep stacks have associated catalogues. These were produced using the standard WFCAM

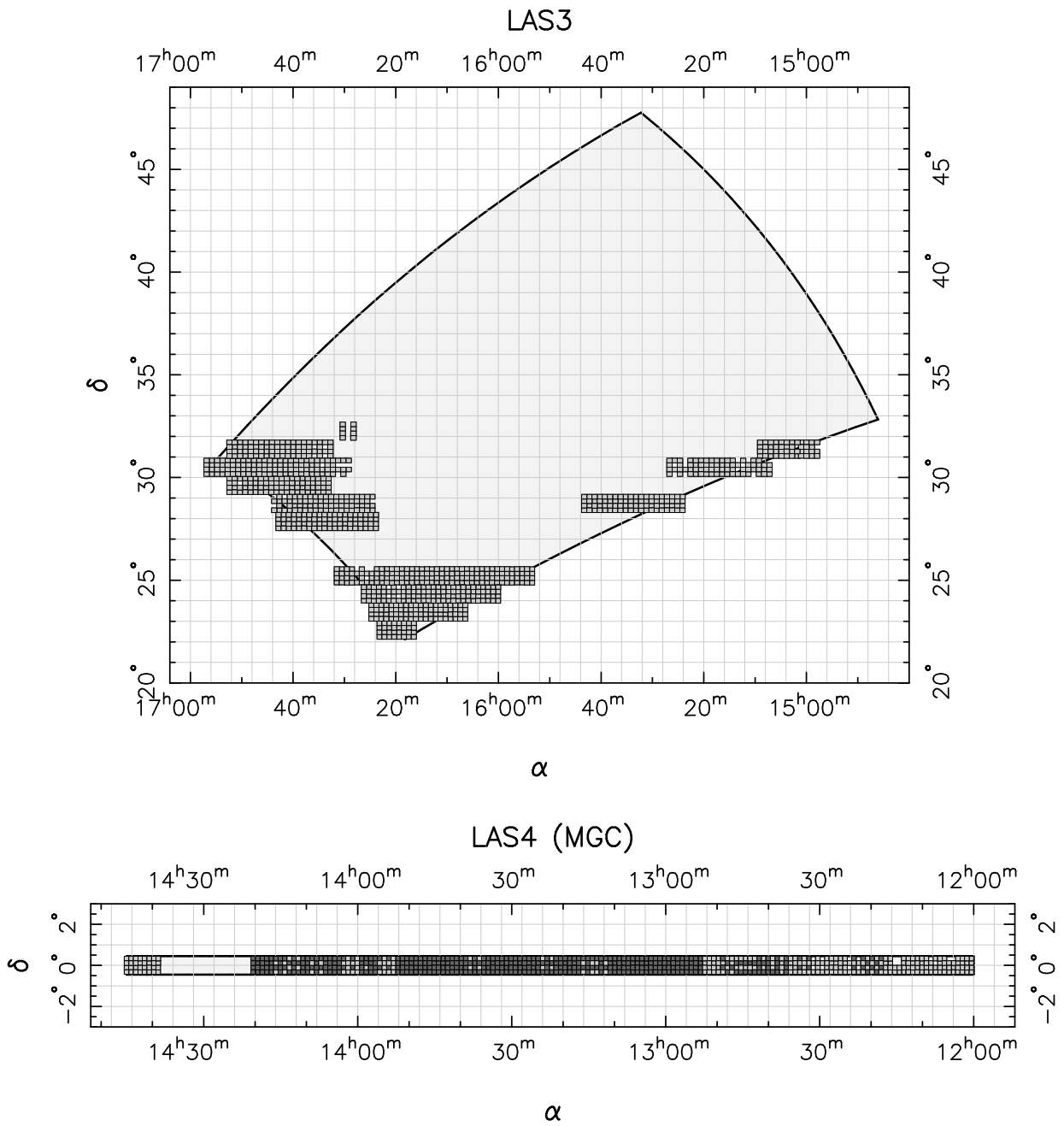

Figure 12. LAS data coverage in the EDR database (all of $YJHK$; dark grey tiles only) and the EDR+ database (light and dark tiles) for projects LAS3 and LAS4. LAS3 is currently only observed in J. Each small square is a detector frame.

pipeline source extractor. For both surveys, calibration was performed by taking bright point sources and calibrating directly to the Leavstack frames. All deep stacks set the extinction to zero since it is meaningless for stacks composed of hundreds of Exposures taken at various airmasses on different nights.

Tables 9 and 10 list the DXS and UDS deep stacks with their respective depths (5σ point source sensitivities). In Figure 10, we plot the last two columns of Table 9 to show how depth in the UKIDSS deep stacks scales with total Integration time.

Caveat

At the present time, we are aware of two unresolved problems affecting the flux errors and magnitude errors in the deep stack data (but not the fluxes or magnitudes themselves). The first relates to co-averaging of the deep stacks in the DXS. The data are represented in integer format and the sky noise is estimated by a k-sigma clipped median estimator. While this works well for shallow stacks, the noise in the deep stacks is often reduced to ~ 1 count (particularly in the J-band). Therefore the measurement becomes unreliable by up to $\sim 20\%$. This leads to the scatter seen in Figure 10 for J.

The second problem relates to the lower limits for the four J-band stacks in Figure 10. These arise due to a safety

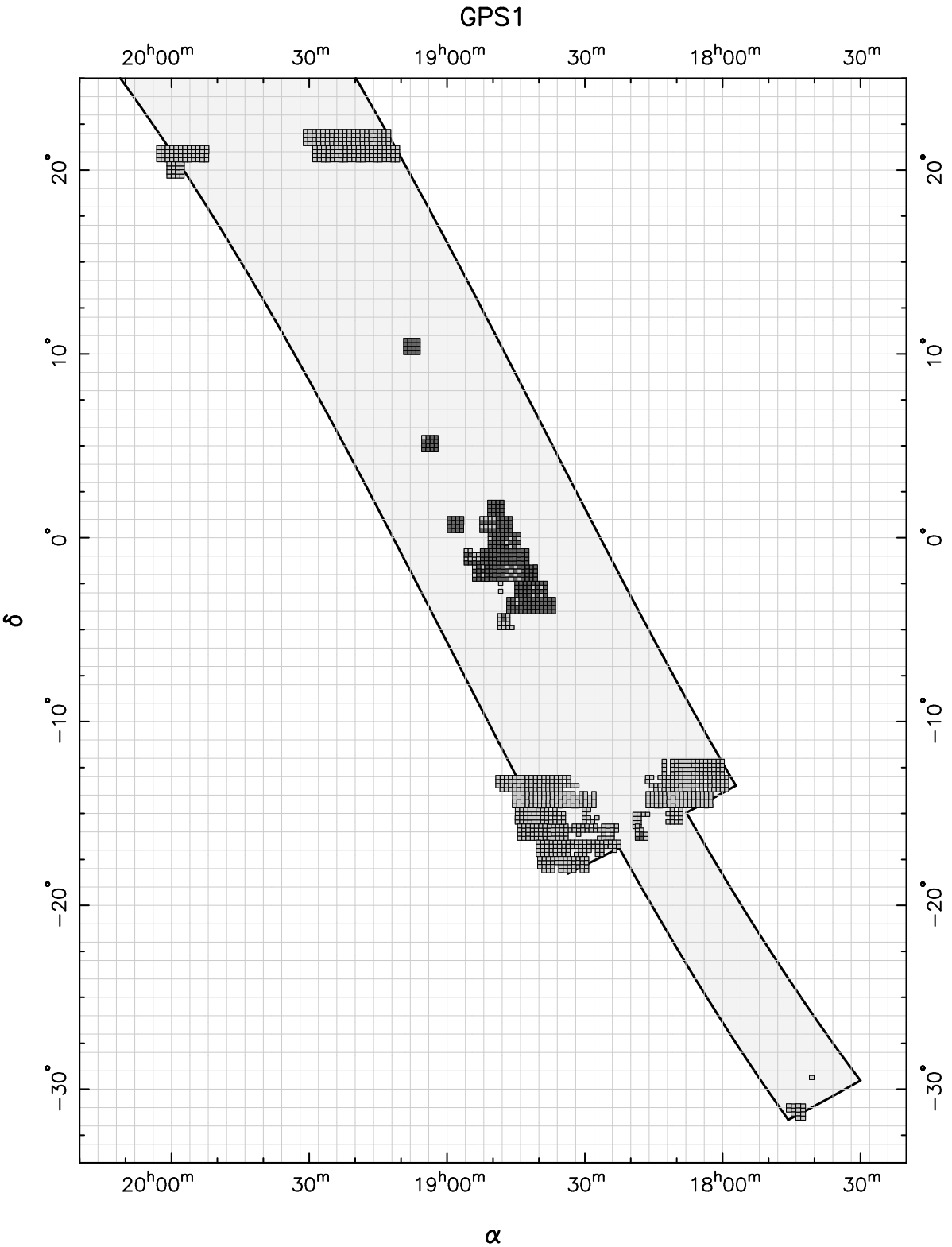

Figure 13. GPS coverage in the EDR database (all of JHK; dark grey tiles) and the EDR+ database (light and dark tiles). Each small square is a detector frame.

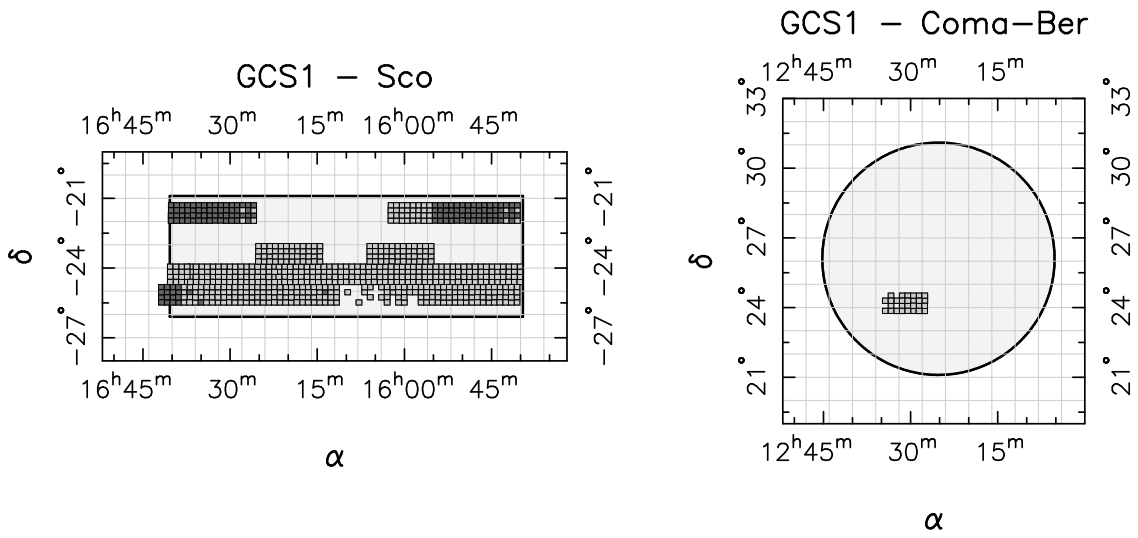

Figure 14. GCS coverage in the EDR database (all of $ZYJHK$; dark grey tiles) and the EDR+ database (light and dark tiles). Each small square is a detector frame.

Region	RA (J2000)	Dec(J2000)	Filter	$t_{\rm int}$ (s)	Depth (mag)
ELAIS N1$^{(\dagger)}$	242.5994000	54.5031333	J	2640.	21.42
ELAIS N1$^{(\dagger)}$	242.5994000	54.7233250	J	4420.	21.64
ELAIS N1$^{(\dagger)}$	242.9817370	54.5031333	J	6060.	21.69
ELAIS N1$^{(\dagger)}$	242.9817370	54.7233250	J	5060.	21.62
ELAIS N1	242.5994000	54.5031333	K	4500.	20.43
ELAIS N1	242.5994000	54.7233250	K	4500.	20.51
ELAIS N1	242.9817370	54.5031333	K	5000.	20.53
ELAIS N1	242.9817370	54.7233250	K	3500.	20.33
Lockman Hole	163.3623000	57.4753556	K	3500.	20.35
Lockman Hole	163.3623000	57.6955472	K	2500.	20.19
Lockman Hole	163.7756167	57.4753556	K	2000.	21.09
Lockman Hole	163.7756167	57.6955472	K	2000.	20.02
XMM-LSS	36.5752020	-4.7496444	J	5760.	22.26
XMM-LSS	36.5803542	-4.5294528	J	6400.	22.28
XMM-LSS	36.8012000	-4.7496444	J	5760.	22.24
XMM-LSS	36.8012000	-4.5294528	J	5760.	22.27
XMM-LSS	36.5752020	-4.7496444	K	6400.	20.83
XMM-LSS	36.5803542	-4.5294528	K	6400.	20.87
XMM-LSS	36.8012000	-4.7496444	K	6400.	20.82
XMM-LSS	36.8012000	-4.5294528	K	3840.	20.62
VIMOS 4	334.2667458	0.1698000	J	8320.	22.21
VIMOS 4	334.2667458	0.3899917	J	10880.	22.38
VIMOS 4	334.4869458	0.1698000	J	9600.	22.36
VIMOS 4	334.4869458	0.3899917	J	5760.	22.18
VIMOS 4	334.2667458	0.1698000	K	9120.	20.82
VIMOS 4	334.2667458	0.3899917	K	12180.	21.00
VIMOS 4	334.4869458	0.1698000	K	10900.	20.95
VIMOS 4	334.4869458	0.3899917	K	9620.	20.97
VIMOS 4	335.1420250	0.1817444	K	7680.	20.90
VIMOS 4	335.1420250	0.4019361	K	8320.	20.91
VIMOS 4	335.3622250	0.1817444	K	8960.	20.92
VIMOS 4	335.3622250	0.4019361	K	8960.	20.88

Table 9. DXS deep stacks. The base co-ordinates, filter, total Integration time in seconds and 5σ point source sensitivity of each multiframe are listed. $^{(\dagger)}$These four J stacks are affected by the sky noise problem discussed in the text – depths quoted are therefore only lower limits.

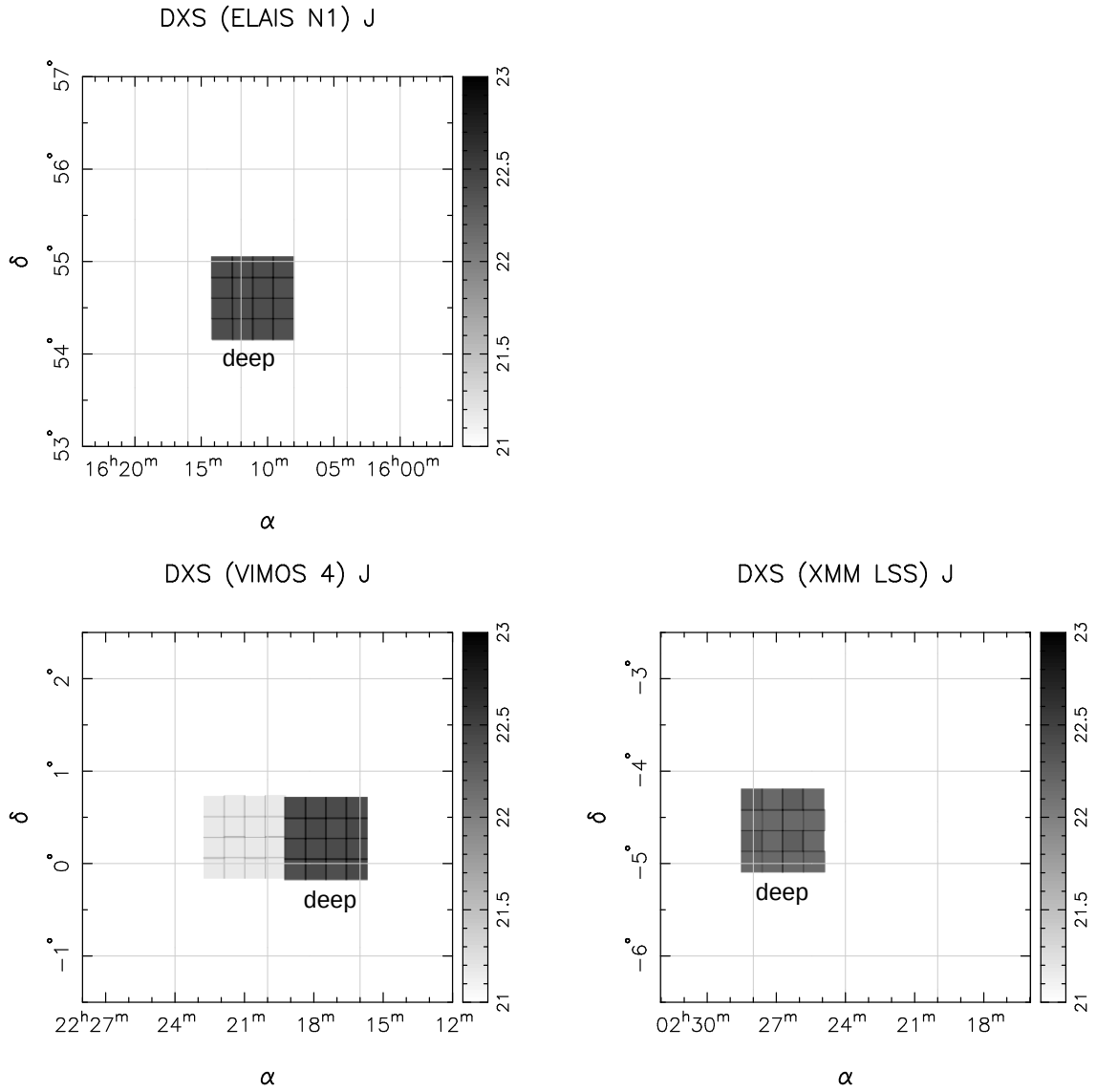

Figure 15. DXS coverage and depth in J. Tiles that are available from the WSA as deep stacks are labelled. Grey-shaded key gives depth in J.

feature in the WFCAM pipeline that sets the sky noise, $\sigma_{\rm sky}$, to $\sigma_{\rm sky} = {\rm MAX}(2.5, \sigma_{\rm sky})$, to prevent it from becoming too low. This gives an over-estimate of the noise and hence an under-estimate of the magnitude limit. This safety feature was removed for catalogues produced from deep stacks, but the four J-band stacks in question contain intermediate stacks where the noise dips below 2.5 counts. The weighting of these four frames is therefore not correct. The affected frames are labelled in Table 9. Note that since the UDS deep stacks were produced independently using SWarp, they are not affected by this problem.

Both problems will be remedied in DR1.

9 THE WFCAM SCIENCE ARCHIVE

In this section we outline the structure of the WSA and describe the means by which data can be obtained by users. The WSA will continue to develop over the course of the 2 year plan. We therefore include details of its current status; upgrades will be announced in future data releases as they occur. We refer the reader to Hambly et al. (2006) for more information.

9.1 WSA architecture

Pipeline processed images and catalogues are held in the WSA, hosted in Edinburgh by WFAU. Image data are stored in the same MEF format produced by the pipeline, with a primary header and one header per extension. The MEFs are referred to as *multiframes*. Catalogues are also stored in the pipeline output MEF format but object data from these are also extracted upon ingest and placed in a relational database running on Microsoft SQL Server 2000.

The multiframe is the principal component of the WSA. The most common multiframe is a pipeline reduced WFCAM observation in a single passband. The WSA refers to

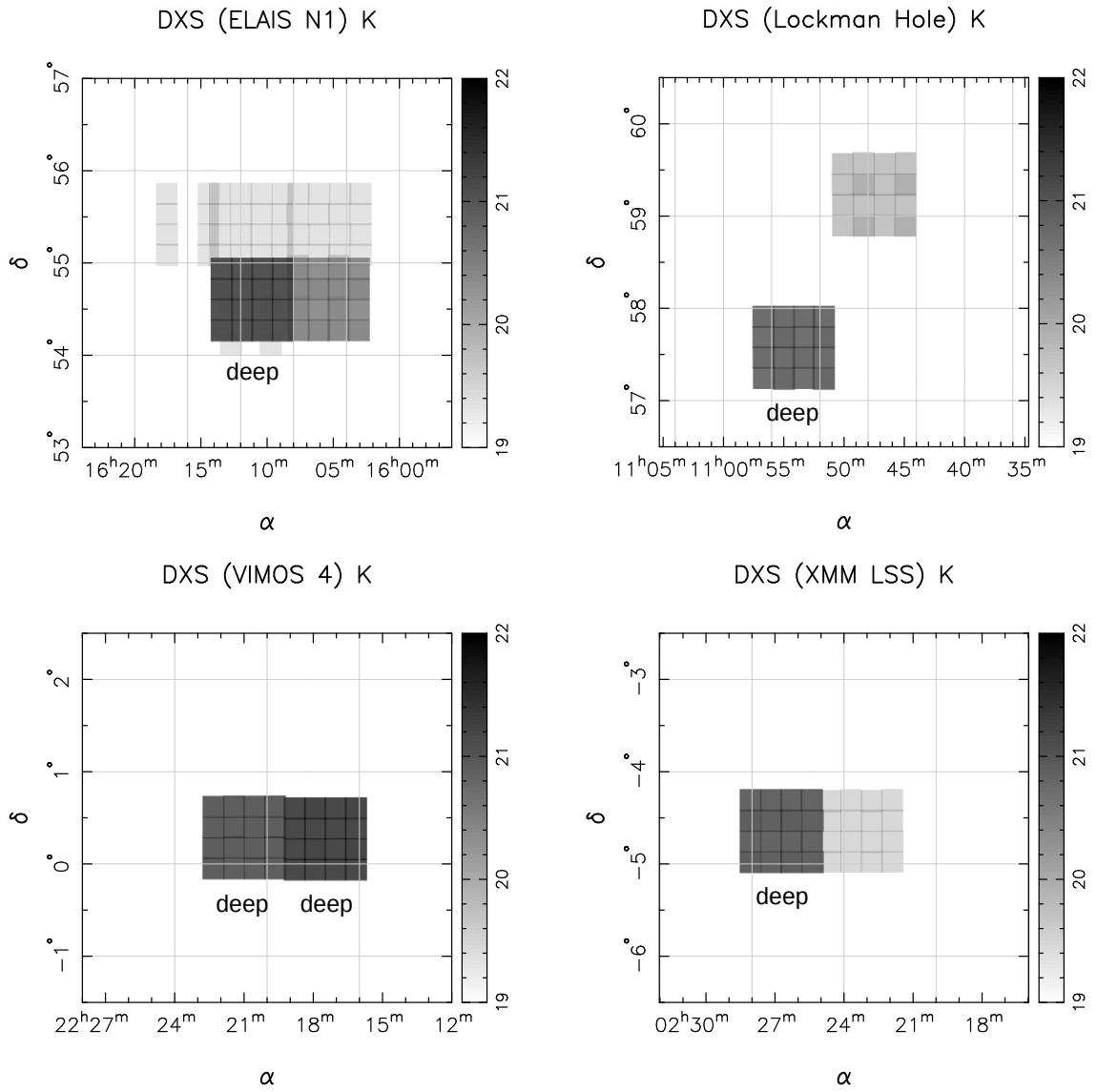

Figure 16. DXS coverage and depth in K. Tiles that are available from the WSA as deep stacks are labelled. Grey-shaded key gives depth in K.

the primary header containing the 'meta-data' (i.e., basic observational details and photometric and astrometric calibrations) of each multiframe as extension 1 (via the attribute `extNum` – see below). Extensions 2 to 5 correspond to the pixel data for detectors 1 to 4 respectively. Multiframes exist for all observation types (e.g., darks, flats, science frames) and data products (e.g., stacks, mosaics and difference images).

Multiframes are described in the database by entries in three main tables. The `Multiframe` table mainly holds the meta-data taken from an MEF's primary header, applicable to the multiframe as a whole. Every multiframe held in the archive is represented by a single row in the multiframe table with attributes (i.e., columns) in the row holding this meta-data. The table `MultiframeDetector` contains details applicable to the individual detector frames that comprise each multiframe. Finally, the third main table, `CurrentAstrometry`, contains the current astrometric calibration coefficients (i.e., the WCS) for each detector frame across all multiframes. `MultiframeDetector` and `CurrentAstrometry` mainly hold information taken from the extension headers of each MEF. A multiframe with four extensions (detectors) gives rise to four corresponding entries (rows) in `MultiframeDetector` and `CurrentAstrometry`.

Each multiframe is assigned a unique ID number, `multiframeID`, which is an attribute in many tables held in the archive including the tables `Multiframe`, `MultiframeDetector` and `CurrentAstrometry`. The `multiframeID` attribute is used, often in conjunction with the extension number attribute, `extNum`, to link the multiframe records held across the tables (see Section 9.2).

Objects extracted from a multiframe by the pipeline are ingested, one object per row, into the corresponding UKIDSS survey *detection table*. All survey detection tables contain the same attributes with each row representing an object detected in one waveband at one epoch. Table A1

Quadrant	RA (J2000)	Dec(J2000)	Filter	$t_{\rm int}$ (s)	Depth
North East	34.7149375	-4.7893583	J	12640.	22.47
North West	34.2424791	-4.7893583	J	12640.	22.28
South East	34.7151208	-5.2923027	J	12640.	22.25
South West	34.2422958	-5.2923027	J	12640.	22.26
North East	34.7149375	-4.7893583	K	20950.	21.11
North West	34.2424791	-4.7893583	K	20950.	21.01
South East	34.7151208	-5.2923027	K	20950.	21.00
South West	34.2422958	-5.2923027	K	20950.	21.10

Table 10. UDS deep stacks. The centre co-ordinates, filter, total Integration time in seconds and 5σ point source sensitivity of each quadrant are listed.

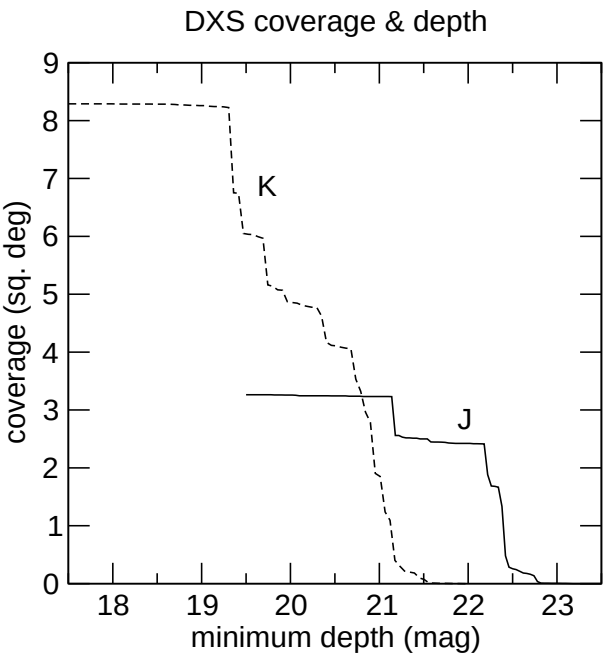

Figure 17. DXS areal coverage attaining a given minimum depth as a function of that minimum depth, for J and K. Depth is the 5σ point source sensitivity, calibrated from the Exposure time using Figure 10.

shows the list of attributes in the detection table. Source merging is carried out by position coincidence matching objects in each survey's detection table to produce that survey's *source table* (see Hambly et al. 2006, for a detailed account of source merging). The source table holds an object's multi-waveband, multi-epoch attributes in one row. Each survey has its own unique source table since each UKIDSS survey requires its own particular set of observations. Table A2 shows the list of attributes in the LAS source table. A log of the source merging for a given survey is recorded in a table `MergeLog`. For efficiency, the attributes held in a source table for an object in a given waveband/epoch is a subset of those recorded in the detection table. To recover the full set of parameters, the attributes `multiframeID`, `frameSetID` and `SeqNum` are provided to allow cross-referencing (see Section 9.2 for some examples). Tables are named by prefixing with the associated three-letter survey abbreviation, for example; `lasDetection`, `lasSource` & `lasMergeLog`.

9.2 WSA access

Access to the WSA is via the following web page:

http://surveys.roe.ac.uk/wsa

The WSA contains data from all pipeline processed WFCAM programmes, both UKIDSS and open time PI programmes. These data have proprietary periods attached to them: UKIDSS data are for use by consortium members and astronomers in ESO member countries for a period of 18 months after release from the archive. Once this proprietary period has expired, access to the data becomes unrestricted. Users wishing to access UKIDSS data who are entitled to do so must register with a UKIDSS EDR community (see UKIDSS website for more details). Once registered, a user may log in to the archive server and gain full access to the pixel and catalogue UKIDSS EDR data.

Note that users must distinguish between the EDR and the EDR+ databases using the drop-down lists. This applies to accessing the menu-driven queries and the 'freeform SQL' interface described below.

9.2.1 Access to pixel data

Pixel data are obtained from the WSA using a menu driven interface. In the first instance, users can obtain details of filter coverage through the 'Archive Listing' interface (in fact, users can also obtain this information via freeform SQL queries – see Section 9.2.2). The Archive Listing interface allows data coverage to be searched by observation type (i.e., object, sky, dark, flat, confidence map and focus image), frame type (i.e., normal, stack, interleave and confidence) and filter. In addition, users can limit searches to a specific UKIDSS survey and if desired, a defined region of sky and range of observation dates. Alternatively, if a user wishes to target a specific multiframe, then its `multiframeID` may be entered. After sending a query from the Archive Listing interface, a table of multiframes is returned. This table lists either a default subset of attributes per multiframe or the complete list, depending on what the user selected. From this table, links direct the user to a JPEG preview of a given multiframe and also to the MEF pixel and catalogue data.

Instead of searching the archive multiframe by multiframe, users can extract cut-out images around a given position via the 'GetImage' and 'MultiGetImage' interfaces. These interfaces currently impose a limit on the size of the cut-out. From GetImage, the limit in practise is the size of a

FITS extension (although in principle is $90' \times 90'$) and from MultiGetImage the limit is $12' \times 12'$. Similar to the Archive Listing interface, the GetImage interface enables users to refine the search by UKIDSS survey, observation type, frame type, filter type or stipulate a specific multiframe. MultiGetImage accepts a list of RA and Dec co-ordinates, currently limited to a maximum of 500. Once a submitted MultiGetImage request is completed, an email is sent to the user containing a link to their results. FITS files and JPEG images are produced and presented in web-page tables and a PDF file. A tar saveset of the FITS files is also generated.

As a demonstration of the flexibility of the WSA, consider the following example combining MultiGetImage with the output returned from an SQL query (see Section 9.2.2). Suppose a user wishes to isolate all potential $z > 7$ QSOs by selecting all objects in the LAS with colours $Y - J > 1.0$ and $0.4 < J - H < 0.8$. Entering the following SQL query into the 'Freeform SQL' interface:

```
SELECT ra,dec
FROM lasSource
WHERE ymj_1Pnt > 2.0
AND j_1mhPnt BETWEEN 0.4 AND 0.8
```

and selecting uncompressed ASCII output returns a list of RA and Dec co-ordinates of objects that satisfies the criteria (here, the point source colours `ymj_1Pnt` and `j_1mhPnt` have been used). After removing header information, this list can then be directly read by the MultiGetImage interface to return FITS images of each candidate object.

9.2.2 Access to catalogue data

Catalogue data are accessed either through freeform SQL queries or menu driven interfaces. When accessing catalogue data, users must distinguish between source tables and detection tables (see Section 9.1). A detection table holds one row for every object detected per stacked multiframe. Therefore, taking the LAS as an example, the same object detected in stacked images in Y, J, H & K will have four separate rows. In the source table, however, this same object would be represented by only one row but with attributes detailing the object's flux in Y, J, H & K. Detection tables are identical between UKIDSS surveys, but source tables, since dependent on survey filter complements, are specific to each survey. Table A1 lists the detection table attributes and Table A2 list attributes in the LAS source table.

The WSA offers three routes of access to the catalogue data (excluding the ability to directly download a MEF catalogue as outlined in Section 9.2.1 via the Archive Listing interface). The first option is a 'Region' search, to search for objects within a specified radius (currently limited to $\leqslant 90'$) from a given co-ordinate. As this option is intended for quick access, here, a user simply has the choice of UKIDSS survey and whether a source or detection table is searched.

A slightly more sophisticated search may be carried out using the 'Menu query' interface, which a user completes in stages. After selecting the relevant UKIDSS survey and source/detection table type, the user is presented with a list of table attributes to be listed per object in the final output. The user selects the relevant attributes as required and is given the option to limit the search within specified limits applied to those attributes. From here, the request can be submitted or, alternatively, the underlying SQL query generated by the menu interface can be edited directly. In this latter case, the generated SQL is passed to the freeform SQL query interface for amendment.

The final option is the freeform SQL interface. This interface is the most powerful, allowing users to access every aspect of the archive. The WSA web pages provide a cook-book for users unfamiliar with SQL. We provide some worked examples here to demonstrate the flexibility of the system.

Example 1: Return YJHK mags and co-ords of objects in a rectangular region in the LAS

This is a basic search that can be carried out with the Menu query interface detailed above, but serves to illustrate some fundamental points. The fact that multi-filter information is required per object from the LAS dictates that the table `lasSource` is required. The SQL to use in this case is (note WSA SQL is case insensitive, capitalisation here is for clarity only):

```
SELECT ra,dec,yAperMag3,j_1AperMag3,
   hAperMag3,kAperMag3
FROM lasSource
WHERE ra BETWEEN 190 AND 191
   AND dec >= -0.5 AND dec <= 0.5
```

All SQL queries start with the `SELECT` statement followed by a list of required attributes. In this example, object co-ordinates and aperture corrected source magnitudes extracted from an $r = 1''$ aperture (`AperMag3` – see Table A1) are chosen (the `j_1AperMag3` signifies the 1st epoch LAS pass in J, `j_2AperMag3` currently contains default values). The second part of a simple SQL select is the `FROM` statement followed by the table name. The `WHERE` clause in the example is optional and is used here to refine the search to a $1^\circ \times 1^\circ$ region within LAS4. Note that both RA and Dec are expressed in decimal degrees and that the SQL `ra BETWEEN 190 AND 191` is identical to the SQL `ra >= 190 AND ra <=191`.

Example 2: Find all K-band detector frames in the GPS with fewer than 10000 detected objects

In this case, the table `MultiframeDetector` must be searched for instances where the number of detected objects, given by the attribute `tableRows`, is < 10000. However, since the query specifically requests only GPS frames and since the necessary attribute `project` is not contained within `MultiframeDetector`, an SQL 'join' with table `Multiframe` containing the `project` attribute must be made. The following SQL achieves this:

```
SELECT M.multiframeID,camNum
FROM MultiframeDetector AS MD, Multiframe AS M
WHERE tableRows < 10000
   AND M.multiframeID = MD.multiframeID
   AND project = "U/UKIDSS/GPS1"
   AND M.filterID=5
   AND frameType LIKE "%stack"
```

Here, both table names are relabelled with the `AS` function to simplify the SQL. To prevent ambiguities, attributes common to both tables, such as `filterID`, must be uniquely specified by prefixing them with the relevant table name, or as in the example above, its relabelled name,

e.g., `M.filterID`. The join is carried out by stipulating `M.multiframeID = MD.multiframeID`. Without this, all instances of stacked GPS K-band multiframes regardless of object detections *and* all detector frames with < 10000 objects within the entire database, regardless of filter or frame type would be returned.

In the example above, the multiframeID and detector number (`camNum` = 1 to 4, not to be confused with `extNum` that runs from 2 to 5) are listed. The `LIKE "%stack"` condition selects all frame types that contain the string 'stack' (i.e., Stack, Leavstack, Deepleavstack etc.), the % acting as a 'match all' wildcard. The `project` attribute identifies the UKIDSS survey name. All UKIDSS survey names in the WSA are prefixed with the (case-insensitive) string "U/UKIDSS/". As mentioned in Section 4, the EDR includes the projects LAS[1-4],GPS1,GCS1,DXS[1-3,_SV] & UDS2. Finally, `filterID` selects the K-band filter, following the WSA convention that `filterID`=1 to 7 respectively corresponds to filters Z, Y, J, H, K, H_2 & $Br\gamma$ (the SQL '`SELECT * FROM Filter`' gives further details).

Example 3: Return the distribution of depth reached in GCS J-band stacked detector frames

In this example, we define depth as the 5σ point source sensitivity limit, given by

$$m_0 - 2.5\log_{10}(5\sigma_{\rm sky}N^{1/2}/t_{\rm exp}) - m_{\rm ap} \qquad (4)$$

where m_0 is the Exposure zero-point, $\sigma_{\rm sky}$ is the pixel-to-pixel standard deviation of background counts in the Exposure, N is the number of pixels within the aperture, $t_{\rm exp}$ is the Exposure time and $m_{\rm ap}$ is the aperture correction. In terms of WSA table attributes, the zero point (from equation 3) is given by `photZPCat` from table `MultiframeDetector`. Since this is computed using $r = 1''$ aperture corrected fluxes (`AperFlux3`), the corresponding aperture correction to use for $m_{\rm ap}$ is `AperCor3` from `MultiframeDetector`. Within an $r = 1''$ aperture, the number of pixels N is given by $\pi/$`xPixSize`^{2}, using `xPixSize` from the table `CurrentAstrometry`. The background noise $\sigma_{\rm sky}$ is given by `skyNoise` from `MultiframeDetector`, but due to inter-pixel covariance in the WFCAM detectors (see Irwin et al. 2006), this must be scaled by $1.2^{1/2}$. Finally, the Exposure time is provided by the attribute `expTime` from `Multiframe`.

Since attributes are used from the tables `Multiframe`, `MultiframeDetector` and `CurrentAstrometry`, a three-way join is needed:

```
SELECT CAST(ROUND(T.depth*10.0,0) AS INT)/10.0
  AS depthBin, COUNT(*)
FROM (
      SELECT photZPCat
        -2.5*LOG10(5.0*skyNoise*
        SQRT(1.2*3.141593)/(xPixSize*expTime))
        -AperCor3 AS depth
      FROM MultiframeDetector AS MFD,
        CurrentAstrometry AS CA,
        Multiframe AS M
      WHERE MFD.MultiframeID=CA.MultiframeID
        AND MFD.extNum=CA.extNum
        AND M.multiframeID=MFD.multiframeID
        AND M.filterID=5
        AND frameType LIKE "%stack"
        AND project = "u/ukidss/gcs1"
      ) AS T
GROUP BY CAST(ROUND(T.depth*10.0,0) AS INT)/10.0
ORDER BY depthBin
```

This is an example of a nested select. The inner select statement returns a table, labelled `T` here, which is then subject to the external select statement. To return a distribution of depths, the above SQL does three things: 1) rounds depths to the nearest 0.1mag with the function `CAST(ROUND(T.depth*10.0,0) AS INT)/10.0`, 2) groups these binned depths together with the `GROUP BY` statement, 3) counts the number of binned depths in each group with `COUNT(*)`. The `ORDER BY` statement simply returns results in order of ascending bin magnitude.

For further examples and more information on access to the WSA, we refer the reader to the WSA Cookbook, Schema Browser and Data Access/Overview via the web address given at the beginning of this section (see also Hambly et al. 2006).

10 SUMMARY

The UKIDSS EDR is the first ESO-wide release of UKIDSS data. The data constitute $\sim 1\%$ of the whole of UKIDSS, but are representative of the expected data quality in future releases. Although this is only a small fraction of what UKIDSS will deliver at the end of its 7-year plan, the EDR is already comparable to the size of 2MASS in terms of the number of photons collected.

The EDR database contains ~ 60 deg^2 of pixel and catalogue data in various combinations of the filter set $ZYJHK$. In addition to the EDR, we have released an extended database, the EDR+, that contains all data in the EDR database plus extra data that have passed QC, but in areas not covered by all of the required filters. The EDR+ database constitutes approximately 215 square degrees.

In this paper, we have described the full data-train, from acquisition to release. We have given some background information to UKIDSS and an overview of the surveys, provided details of the observational implementation, outlined our quality control and calibration procedures, quantified the quality of the image and catalogue data and finally given instructions and worked examples for access to the WSA.

The first large release of UKIDSS data to the ESO community, DR1, will occur in summer 2006. We refer the reader to the UKIDSS website (*http://www.ukidss.org*) for news and progress updates.

Acknowledgements

SD thanks the U.K. Particle Physics and Astronomy Research Council for 6 months funding as Consortium Science Verifier.

REFERENCES

Bertin, E., Mellier, Y., Radovich, M., Missonnier, G., Didelon, P., Morin, B., 2002, '*Astronomical Data Analysis Software and Systems XI*', ASP Conference Proceedings, Vol.

281, p. 228. Eds. D. A. Bohlender, D. Durand, & T. H. Handley.
Casali, M., et al., 2006, in prep.
Churchwell, E. B., et al., 2002, AAS, 201, 5006
Cutri, R. M., et al., 2003, Explanatory Supplement to the 2MASS All Sky Data Release, IPAC
Hambly, N. C., et al., 2006, in prep.
Hawarden, T. G., Leggett, S. K., Letawsky, M. B., Ballantyne, D. R.; Casali, M. M., 2001, MNRAS, 325, 563
Hewett, P. C., Warren, S. J., Leggett, S. K., Hodgkin, S. T., MNRAS in press
Hodgkin, S. T., et al., 2006, MNRAS, in prep.
Irwin, M. J. & Trimble, V., 1984, AJ, 89, 83
Irwin, M. J., 1985, MNRAS, 214, 575
Irwin, M. J., et al. 2006, in prep.
Lawrence, A., et al., 2006, MNRAS, in prep.
Liske, J., Lemon, D. J., Driver, S. P., Cross, N. J. G., Couch, W. J., 2003, MNRAS, 344, 307
Nikolaev, S., Weinberg, M. D., Skrutskie, M. F., Cutri, R. M., Wheelock, S. L., Gizis, J. E., Howard, E. M., 2000, AJ, 120, 3340
Tokunaga, A. T., Simons, D. A. & Vacca, W. D., 2002, PASP, 114, 180

APPENDIX A: TABLES OF CONTENTS OF THE WSA

For orientation, we tabulate the attributes found in all WSA detection tables (Table A1) and, as an example since they are survey specific, the attributes in the `lasSource` table (Table A2). For more complete and up-to-date information, users should refer to the online versions of these tables found in the WSA schema browser under the web address *http://surveys.roe.ac.uk/wsa*.

Name	Unit	Description
multiframeID		Unique UD (UID) of the relevant multiframe
extNum		Extension number of the multiframe
cuEventID		UID of curation event giving rise to this record
seqNum		Running number of this detection
filterID		UID of combined filter (assigned in WSA)
isoFlux	ADU	Instrumental isophotal flux counts
isoMag	mag	Calibrated isophotal magnitude
x	pix	X coordinate of detection
xErr	pix	Error in X coordinate
y	pix	Y coordinate of detection
yErr	pix	Error in Y coordinate
gauSig	pix	RMS of axes of ellipse fit
ell		1-b/a, where a,b=semi-major,-minor axis
pa	deg	Orientation of ellipse fit to x axis
aProf[1-8]	pix	No. pixels above a series of thresholds relative to local sky
pHeight	ADU	Highest pixel value above sky
pHeightErr	ADU	Error in peak height
aperFlux[1-13]	ADU	Aperture fluxes of diameter D= $2^{(n-1)/2}$ arcsec, $n = 1, 13$
aperFlux[1-13]err	ADU	Error in aperture fluxes [1-13]
aperMag[1-13]	mag	Calibrated aperture corrected aperture magnitudes [1-13]
aperMag[1-13]err	mag	Error in calibrated aperture magnitudes [1-13]
petroRad	pix	Petrosian radius r_p, defined in Yasuda et al. 2001 AJ 112 1104
kronRad	pix	Kron radius r_k, defined in Bertin and Arnouts 1996 A&A Supp 117 393
hallRad	pix	Hall radius r_h, e.g., Hall & Mackay 1984 MNRAS 210 979
petroFlux	ADU	Petrosian flux within circular aperture to $2r_p$
petroFluxErr	ADU	Error on Petrosian flux
petroMag	mag	Calibrated magnitude from Petrosian flux
petroMagErr	mag	Error on calibrated Petrosian magnitude
kronFlux	ADU	Kron flux within circular aperture to $2r_k$
kronFluxErr	ADU	Error on Kron flux
kronMag	mag	Calibrated Kron magnitude from Kron flux
kronMagErr	mag	Error on calibrated Kron magnitude
hallFlux	ADU	Hall flux within circular aperture to $2r_h$: Alternative total flux
hallFluxErr	ADU	Error on Hall flux
hallMag	mag	Calibrated magnitude from Hall flux
hallMagErr	mag	Calibrated error on Hall magnitude
errBits		Processing warning/error bitwise flags
sky	ADU	Local interpolated sky level from background tracker
skyVar	ADU	Local estimate of variation in sky level around image
deblend		Flag for parent of deblended deconstruct (redundant; only deblended images kept)
ra	deg	Celestial Right Ascension
dec	deg	Celestial Declination
cx		Unit vector of spherical co-ordinate
cy		Unit vector of spherical co-ordinate
cz		Unit vector of spherical co-ordinate
htmID		HTM index (20 digits) for equatorial co-ordinates
l	deg	Galactic longitude
b	deg	Galactic latitude
lambda	deg	SDSS system spherical co-ordinate 1
eta	deg	SDSS system spherical co-ordinate 2
class		Flag indicating most probable morphological classification
classStat		N(0,1) stellarness-of-profile statistic
psfFlux	ADU	PSF-fitted flux (****not currently implemented****)
psfFluxErr	ADU	Error on PSF-fitted flux (****not currently implemented****)
psfMag	mag	PSF-fitted calibrated magnitude (****not currently implemented****)
psfMagErr	mag	Error on PSF-fitted calibrated magnitude (****not currently implemented****)
psfFitX	pix	PSF-fitted X coordinate (****not currently implemented****)
psfFitXerr	pix	Error on PSF-fitted X coordinate (****not currently implemented****)
psfFitY	pix	PSF-fitted Y coordinate (****not currently implemented****)
psfFitYerr	pix	Error on PSF-fitted Y coordinate (****not currently implemented****)
psfFitChi2		standard normalised variance of PSF fit (****not currently implemented****)
psfFitDof		No. degrees of freedom of PSF fit (****not currently implemented****)

Table A1. List of parameters in the WSA detection table. Note that at the present time, PSF fitted fluxes and Sersic fluxes are not implemented. WSA attributes for these fluxes currently contain default values.

Name	Unit	Description
SerFlux1D	ADU	1D Sersic flux (**not currently implemented**)
SerMag1D	mag	Calibrated 1D Sersic flux (**not currently implemented**)
SerScaleLen1D		Sersic scale length (**not currently implemented**)
SerIdx1D		Power law index (**not currently implemented**)
SerFit1DChi2		Error in 1D fit (**not currently implemented**)
SerFitNu1D		1D Sersic fit nu (**not currently implemented**)
SerFlux2D	ADU	2D Sersic flux (**not currently implemented**)
SerMag2D	mag	Calibrated 2D Sersic flux (**not currently implemented**)
SerScaleLen2D		Scale length (**not currently implemented**)
SerIdx2D		Power law index (**not currently implemented**)
SerFit2DChi2		Error in 2D fit (**not currently implemented**)
SerFitNu2D		2D Sersic fit nu (**not currently implemented**)
ppErrBits		Additional WFAU post-processing error bits (currently a place holder)
deprecated		Code for a current (=0) or deprecated (!=0) detection
objID		Unique identifier for this detection

Table A1 – *continued* List of parameters in the WSA detection table.

Name	Unit	Description
sourceID		UID of merged detection
cuEventID		UID of curation event giving rise to this record
frameSetID		UID of the set of frames that this merged source comes from
ra	Degrees	Celestial Right Ascension
dec	Degrees	Celestial Declination
sigRa	Degrees	Uncertainty in RA
sigDec	Degrees	Uncertainty in Dec
epoch	Years	Epoch of position measurement
muRa	mas/yr	Proper motion in RA direction
muDec	mas/yr	Proper motion in Dec direction
sigMuRa	mas/yr	Error on proper motion in RA direction
sigMuDec	mas/yr	Error on proper motion in Dec direction
chi2		Chi-squared value of proper motion solution
nFrames		No. of frames used for this proper motion measurement
cx		unit vector of spherical co-ordinate
cy		unit vector of spherical co-ordinate
cz		unit vector of spherical co-ordinate
htmID		HTM index, 20 digits, for co-ordinate
l	Degrees	Galactic longitude
b	Degrees	Galactic latitude
lambda	Degrees	SDSS system spherical co-ordinate 1
eta	Degrees	SDSS system spherical co-ordinate 2
priOrSec		Seam code for a unique (=0) or duplicated (!=0) source (i.e., overlap duplicates)
ymj_1Pnt	mag	Point source colour Y-J
ymj_1PntErr	mag	Error on point source colour Y-J
j_1mhPnt	mag	Point source colour J-H
j_1mhPntErr	mag	Error on colour J-H
hmkPnt	mag	Point source colour H-K
hmkPntErr	mag	Error on point source colour H-K
ymj_1Ext	mag	Extended source colour Y-J
ymj_1ExtErr	mag	Error on extended source colour Y-J
j_1mhExt	mag	Extended source colour J-H
j_1mhExtErr	mag	Error on extended source colour J-H
hmkExt	mag	Extended source colour H-K
hmkExtErr	mag	Error on extended source colour H-K
mergedClassStat		Merged N(0,1) stellarness-of-profile statistic
mergedClass		Class (1|0| − 1| − 2| − 3| − 9=galaxy|noise|stellar|probableStar|probableGalaxy|saturated)
pStar		Probability that the source is a star
pGalaxy		Probability that the source is a galaxy
pNoise		Probability that the source is noise
pSaturated		Probability that the source is saturated
yHallMag	mag	Point source Y mag
yHallMagErr	mag	Error in point source Y mag
yPetroMag	mag	Extended source Y mag (Petrosian)
yPetroMagErr	mag	Error in extended source Y mag (Petrosian)
yPsfMag real	mag	Point source profile-fitted Y mag
yPsfMagErr	mag	Error in point source profile-fitted Y mag
ySerMag2D	mag	Extended source Y mag (profile-fitted)
ySerMag2DErr	mag	Error in extended source Y mag (profile-fitted)
yAperMag3	mag	Extended source Y mag (2.0 arcsec aperture diameter)
yAperMag3Err	mag	Error in extended source Y mag (2.0 arcsec aperture diameter)
yAperMag4	mag	Extended source Y mag (2.8 arcsec aperture diameter)
yAperMag4Err	mag	Error in extended source Y mag (2.8 arcsec aperture diameter)
yAperMag6	mag	Extended source Y mag (5.7 arcsec aperture diameter)
yAperMag6Err	mag	Error in extended source Y mag (5.7 arcsec aperture diameter)
yGausig	pixels	RMS of axes of ellipse fit in Y
yEll		1-b/a, where a/b=semi-major/minor axes in Y
yPA	Degrees	Ellipse fit celestial orientation in Y
yErrBits		Processing warning/error bitwise flags in Y
yDeblend		Flag indicating parent/child relation in Y

Table A2. List of parameters in the LAS source table. Note that attributes yHallMag to yEta repeat for each of j_1, j_2, h & k – these are omitted here for brevity. Currently, all attributes relating to proper motion contain default values.

Name	Unit	Description
`yClass`		Discrete image classification flag in Y
`yClassStat`		N(0,1) stellarness-of-profile statistic in Y
`yppErrBits`		Additional WFAU post-processing error bits in Y
`ySeqNum`		Running number of the Y detection
`yObjID`		UID of the Y detection
`yXi`	arcsec	Offset of Y detection from master position (+east/-west)
`yEta`	arcsec	Offset of Y detection from master position (+north/-south)

Table A2 – *continued* List of parameters in the LAS source table.